
REVISITING DEEP ENSEMBLE FOR OUT-OF-DISTRIBUTION DETECTION: A LOSS LANDSCAPE PERSPECTIVE

Kun Fang¹, Qinghua Tao², Xiaolin Huang¹ and Jie Yang¹

¹Department of Automation, Shanghai Jiao Tong University, {fanghenshao, xiaolinhuang, jieyang}@sjtu.edu.cn

²ESAT-STADIUS, KU Leuven, Belgium, qinghua.tao@esat.kuleuven.be

ABSTRACT

Existing Out-of-Distribution (OoD) detection methods address to detect OoD samples from In-Distribution data (InD) mainly by exploring differences in features, logits and gradients in Deep Neural Networks (DNNs). We in this work propose a new perspective upon *loss landscape* and *mode ensemble* to investigate OoD detection. In the optimization of DNNs, there exist many local optima in the parameter space, or namely *modes*. Interestingly, we observe that these independent modes, which all reach low-loss regions with InD data (training and test data), yet yield significantly different loss landscapes with OoD data. Such an observation provides a novel view to investigate the OoD detection from the loss landscape and further suggests significantly fluctuating OoD detection performance across these modes. For instance, FPR values of the RankFeat [1] method can range from 46.58% to 84.70% among 5 modes, showing uncertain detection performance evaluations across independent modes. Motivated by such diversities on OoD loss landscape across modes, we revisit the deep ensemble method for OoD detection through mode ensemble, leading to improved performance and benefiting the OoD detector with reduced variances. Extensive experiments covering varied OoD detectors and network structures illustrate high variances across modes and also validate the superiority of mode ensemble in boosting OoD detection. We hope this work could attract attention in the view of independent modes in the OoD loss landscape and more reliable evaluations on OoD detectors.

Keywords Out-of-distribution detection · Loss landscape · Mode · Ensemble

1 Introduction

For years Deep Neural Networks (DNNs) have shown powerful abilities in fitting In-Distribution (InD) data. Given a DNN f well-trained on data from some distribution \mathcal{P}_{in} , f also performs well on the test data, which is commonly regarded as being from the same distribution \mathcal{P}_{in} as the training data [2]. However, the generalization ability of f on the data from an out-distribution \mathcal{P}_{out} is still prohibitive, which brings a large number of researches [3, 4, 5, 6, 7, 8, 9, 1, 10, 11, 12, 13] trying to detect Out-of-Distribution (OoD) samples in the inference stage, known as the popular OoD detection problem [14, 15].

In the existing works for OoD detection, the key is to find the different responses from DNNs towards InD and OoD data and then to leverage such differences to distinguish OoD samples. There are different ways to measure such differences with DNNs, such as the logits or probabilities [3, 4, 6, 12], the features or activations [5, 8, 1, 10, 11, 12, 13], the parameter gradients [7, 9], etc. For example, an early work MSP [3] directly uses the maximum softmax probability to detect the abnormal predictive confidence from DNNs on OoD data. GradNorm [9], as its name suggests, uses the norm of the gradients as the detection metric, since the gradients of InD and OoD data are distinctively different *w.r.t* the carefully-designed loss in the paper. A recent work RankFeat [1] proposes to remove the rank-1 feature matrix in the forward propagation during inference, as the rank-1 matrix is the mostly likely to contain information causing the over-confidence of OoD predictions.

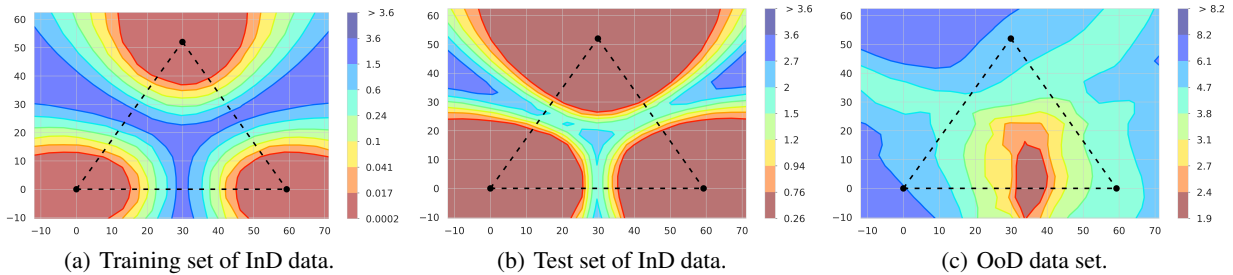


Figure 1: An illustration on the loss landscape of InD and OoD data, as a function of network weights in a two-dimensional subspace. The 3 isolated modes are located in similar low loss regions on the InD data, but in significantly different loss areas for the OoD data. The visualization technique follows [16]. Refer to Fig.4 for more details on each mode.

In this work, we address the OoD detection problem from a novel perspective: *loss landscape* and *mode ensemble*. The loss landscape of DNNs is extremely complex and highly non-convex due to the millions of parameters and non-linear activations, which inevitably results in numerous isolated optima (*modes*) in the loss landscape, suggest by lots of pioneering works [17, 16, 18, 19]. Nevertheless, these works all focus on mode properties in the loss landscape of in-distribution data. By introducing the loss landscape of OoD data and visualizing locations of 3 isolated modes in Fig.1 and Fig.4, we observe a key phenomenon on those isolated modes that are trained independently on InD data *w.r.t* different random seeds: These modes, even though located in isolation in the loss landscape, undoubtedly all reach low-loss regions on the InD data, shown in Fig.1(a) and Fig.1(b), yet, their locations in the loss landscape for the OoD data instead hold strong diversities, *i.e.*, these modes show significantly distinct loss regions for the OoD data, shown in Fig.1(c) and Fig.4 with more details.

Considering such diversities of these modes in the OoD loss landscape, there naturally exists a hypothesis that these independent modes, though all with consistently good performance on InD data, might hold a large variance on the OoD detection results even under the same OoD detector. For example, in Fig.2, the RankFeat method achieves fluctuating FPR values ranging from 46.58% to 84.70% among different modes of the same network structure on the same OoD data set. Besides, detection results between 2 OoD detectors could be opposite on different modes, *e.g.*, RankFeat outperforms Energy on mode3 but falls inferior on mode1 and mode2. Such high detection variances among independent modes have been ignored by the research community and bring difficulties in developing and evaluating OoD detectors.

All these findings hence motivate us to explore OoD detection across independent modes, rather than within a single mode, to leverage the diversities reflected on the OoD loss landscape. Accordingly, we revisit the deep ensemble method [20] to perform mode ensemble for OoD detection, which is shown to bring substantial variance reduction and performance improvements and help the evaluation on OoD detectors. Specifically, for different types of OoD detectors, we design corresponding mode ensemble strategies by ensembling the output logits or features from multiple isolated modes, then the ensembled outputs are exploited by those OoD detectors. Besides, a theoretical derivation is provided to show the superiority of ensembling modes over the average of single modes. Our experiments for mode ensemble are extensive and comprehensive: (i) Various state-of-the-art (SOTA) OoD detection methods are involved, including logits-, features- and gradients-based detectors; (ii) Small-scale, large-scale data sets and distinct network architectures, including the prevailing vision transformer (ViT, [21]), are covered. All these theoretical and empirical results support our viewpoint: there exist high variances in OoD detection performance of independent modes, and mode ensemble could bring substantial performance improvements and help the evaluation of OoD detectors, which we hope could benefit the research community with the perspective of independent modes in the OoD loss landscape.

Our contributions are summarized as follows:

- We propose a novel perspective, *loss landscape* and *mode ensemble*, to analyze and address the OoD detection problem. Our observation shows that isolated modes hold diversified loss landscapes on OoD data, resulting in high variances of OoD detection results among these modes.
- We revisit the deep ensemble method to perform mode ensemble, design corresponding ensemble strategies for different types of OoD detectors, and find more stable and better OoD detection results.
- Extensive and comprehensive empirical results including ablation studies and comparisons with other ensemble methods have verified the uncertainties of single modes and advantages of mode ensemble in the OoD detection task.

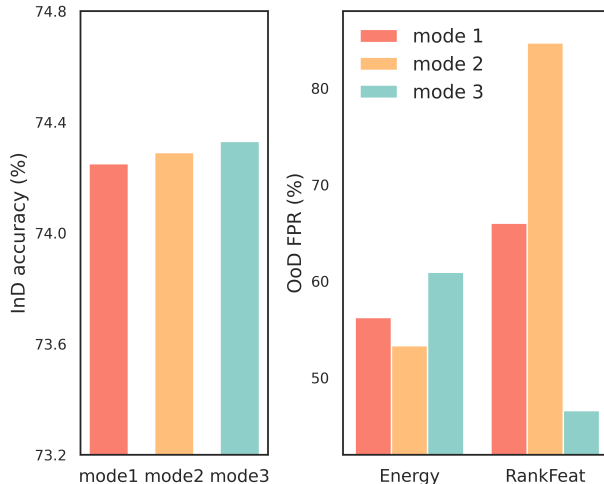


Figure 2: There exists a high variance among the OoD detection results (FPR95) of the 3 modes on 2 OoD detectors Energy [6] and RankFeat (the right panel), while the 3 modes all hold good and similar recognition accuracy on the InD test set (the left panel).

In the following, Sec.2 elaborates our mode ensemble method for OoD detection. Experiments are presented in Sec.3 and related works are shown in Sec.4. Sec.5 finally draws conclusions and discussions.

2 OoD detection with ensemble modes

In this section, we firstly outline the background of OoD detection in Sec.2.1, then give detailed elaboration on the loss landscape and mode ensemble of our method in Sec.2.2, and provide theoretical analysis in Sec.2.3.

2.1 Preliminary: OoD detection

Given a neural network $f : \mathbb{R}^D \rightarrow \mathbb{R}^C$, its training data is from some distribution \mathcal{P}_{in} , known as the in-distribution. Once deployed, f will encounter unseen data that could be from either the known distribution \mathcal{P}_{in} or an unknown out-distribution \mathcal{P}_{out} . OoD detection aims at deciding whether one new test sample $\mathbf{x} \in \mathbb{R}^D$ is from \mathcal{P}_{in} or \mathcal{P}_{out} .

Generally, OoD detection is formulated as a binary classification problem with a decision function $D(\cdot)$ and a scoring function $S(\cdot)$:

$$D(\mathbf{x}) = \begin{cases} \text{InD}, & S(\mathbf{x}) > \lambda, \\ \text{OoD}, & S(\mathbf{x}) < \lambda. \end{cases} \quad (1)$$

The scoring function $S(\cdot)$ gives a score for the test sample \mathbf{x} . If the score $S(\mathbf{x})$ is greater than a threshold λ , then \mathbf{x} will be viewed as an InD sample by the decision function $D(\cdot)$, and vice versa. λ is appropriately chosen so that a large proportion (e.g., 95%) of InD data will be correctly classified. A reasonable and justified scoring function $S(\cdot)$ is the key to successfully distinguish OoD data from InD data.

2.2 Mode ensemble for OoD detection

2.2.1 Loss landscape

Inspired by prior works investigating the loss landscape and mode connectivity for the generalization ability of DNNs on the InD test data [17, 16, 18, 19], we propose to analyze the OoD detection problem from the loss landscape perspective. Specifically, our analysis focuses on those *independent* or *isolated* modes that are obtained by training multiple DNNs merely on the InD data *w.r.t* different random seeds. As the random seed dominates the DNN initialization and the noise in SGD optimization, these modes are actually in correspondence to different training trajectories, and thus are independent and isolated. Fig.3 illustrates 3 different trajectories of the learned features during training *w.r.t* 3 different random seeds.

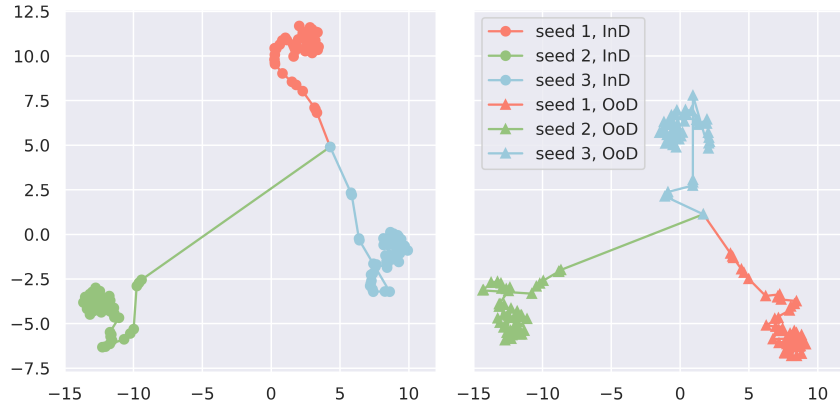


Figure 3: An illustration on the feature trajectories *w.r.t* 3 different random seeds during training on CIFAR10 (InD). 48 checkpoints in each training are sampled. The learned features of CIFAR10 (left) and LSUN (OoD, right) by these checkpoints are reduced to 2-dimension via t-SNE [22] for visualization, showing clearly the resulting 3 isolated modes.

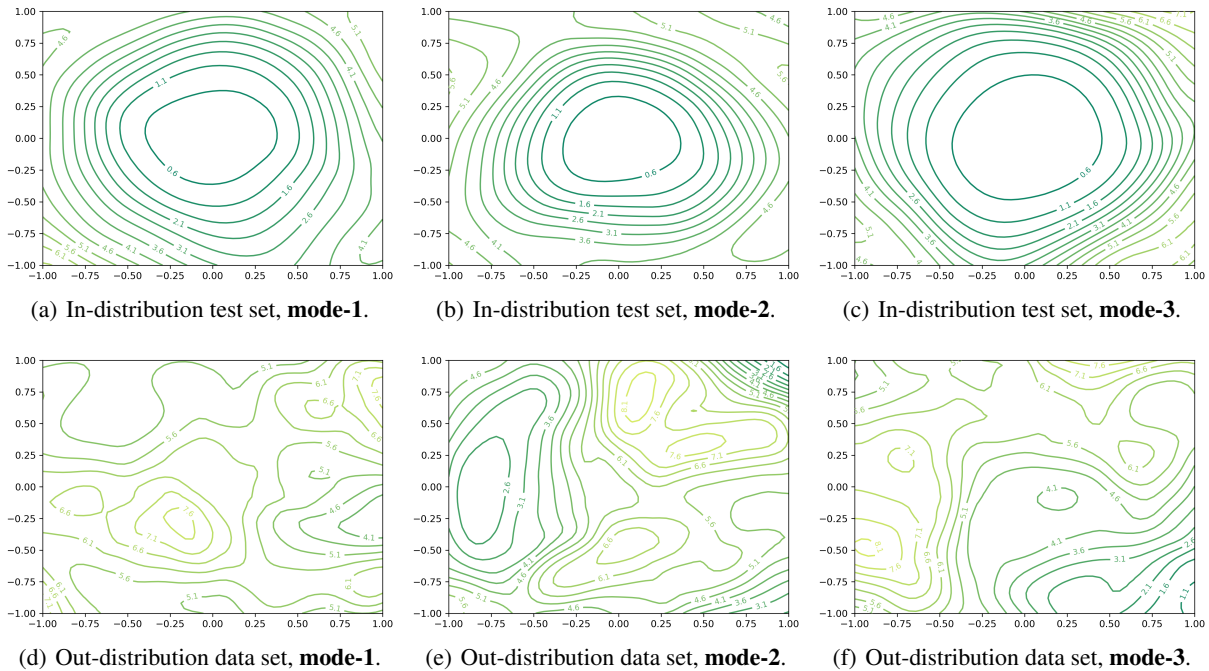


Figure 4: An illustration of the loss landscapes of 3 independent modes (left, middle and right, respectively) on the InD (top) and OoD (bottom) data. The visualization technique follows [23].

As these modes are well-trained on the InD data, though they are independent and isolated with each other, their locations in the loss landscape of InD data still share similarities, *i.e.*, low-loss regions of the InD data. However, for the unseen data from an *out* distribution, these modes might be located in distinctive positions with either high or low losses on the OoD data. In Fig.4, as a complement to Fig.1, the loss landscapes of each mode on the InD and OoD data are visualized, and there clearly exist notable differences in the OoD loss landscapes among those independent modes.

Accordingly, the diversities on the loss landscapes (Fig.4) and features (Fig.3) among the independent modes inspire us to investigate the OoD detection problem across such modes. As the existing OoD detectors mainly focus on one single mode and rely on the differences in the logits or features between InD and OoD data, a hypothesis naturally comes to the mind:

The OoD detection performance of one single mode is of high uncertainty, since such a mode, well-trained on InD data, is possibly located in diverse positions of significantly different loss landscapes of OoD data.

Our experiments in the Sec.3 and *supplementary material* further validate this hypothesis, *i.e.*, the high variances of the OoD detection performance among independent modes.

Such a phenomenon has not been explored by the research community. The high variances among independent modes hinder the development and evaluation on OoD detectors. Besides, we hope our work could benefit the OoD detection researches from the perspective of independent modes in the loss landscape, as an alternative choice aside from exploiting the outputs of single DNNs.

2.2.2 Mode ensemble

To further exploit such diversities on the OoD loss landscape and to reduce the high variances across modes, we revisit the deep ensemble method [20], leverage multiple independent modes to perform mode ensemble, and find significant variance reduction with substantial performance improvements in OoD detection.

Nevertheless, how to efficiently involve various OoD detection methods into the mode ensemble framework remains a troublesome issue. On the one hand, as pointed in [24], directly ensembling the “yes or no” detection results from multiple single modes will accumulate the misclassification probabilities. On the other hand, current detectors work on different outputs of DNNs, including logits, features and gradients, which indicates that the mode ensemble should be carefully designed for specific detectors.

Given N modes $f_{s_1}, \dots, f_{s_N} \in \mathbb{R}^D \rightarrow \mathbb{R}^C$ trained independently *w.r.t* N random seeds s_1, \dots, s_N , in this work, the mode ensemble during inference takes a general form as:

$$\mathbf{h}_{\text{ens}} = \frac{1}{N} \sum_{i=1}^N \mathbf{h}_{s_i}, \quad (2)$$

where \mathbf{h}_{s_i} denotes the output features or logits from f_{s_i} . Such ensembled features or logits \mathbf{h}_{ens} from multiple isolated modes are then exploited by different OoD detectors to achieve mode ensemble for OoD detection. We put complete and thorough details of the mode ensemble for those representative OoD detectors in the *supplementary material*. In this work, we mainly focus on those *post-hoc* and *OoD-agnostic* detectors, covering all aforementioned 3 types, since such detectors do not require OoD data or additional model modifications during training and execute detection strategies only in the inference stage.

Discussions with other ensemble methods for OoD detection [25, 26, 24] Among these works, [25] requires training DNNs with a margin loss involving additional OoD data, which is orthogonal to our settings that models trained solely on InD data are considered. [26] introduces the contrastive loss and the triplet loss to train Siamese networks and triplet networks for ensemble, where the trained networks are not independent with each other. In [24], a novel p-value-based ensemble strategy is proposed for detecting OoD samples, which differs from the common threshold-based decision rule. Our loss landscape perspective motivates us to focus on the general case: standard models trained without OoD data, in correspondence to those *post-hoc*, *OoD-agnostic* and *model-agnostic* OoD detectors. Besides, the comparisons with those existing ensemble methods for OoD detection can be found in the *supplementary material*.

2.3 Theoretical analysis

In this section, we provide a theoretical discussion on how ensemble boosts OoD detection performance. Our analysis follows the setups in [27] and shows the superiority of ensembling modes over the average of single modes in terms of accuracy difference between InD data and OoD data.

Let us consider a binary classification problem and suppose the in-distribution \mathcal{P}_{in} is an isotropic Gaussian:

$$\mathcal{P}_{\text{in}} = \{(\mathbf{x}, y) \mid \mathbf{x} \sim \mathcal{N}(\boldsymbol{\mu} \cdot y; \sigma^2 I_{D \times D})\}, \quad (3)$$

where $\mathbf{x} \in \mathbb{R}^D$, $y \in \{-1, 1\}$, $\boldsymbol{\mu} \in \mathbb{R}^D$ is the mean vector and variance $\sigma^2 > 0$. The out-distribution \mathcal{P}_{out} is defined as a shift from \mathcal{P}_{in} :

$$\mathcal{P}_{\text{out}} = \{(\mathbf{x}, y) \mid \mathbf{x} \sim \mathcal{N}(\boldsymbol{\mu}' \cdot y; \sigma'^2 I_{D \times D}), \boldsymbol{\mu}' = \alpha \cdot \boldsymbol{\mu} + \beta \cdot \boldsymbol{\Delta}, \quad \sigma' = \gamma \cdot \sigma\}, \quad (4)$$

where $\alpha, \beta, \gamma > 0$ are fixed scalars and $\boldsymbol{\Delta} \in \mathbb{R}^D$ is an unknown random distribution.

For mode ensemble, we consider N linear classifiers in the form of $g_i : \mathbf{x} \rightarrow \text{sign}(\boldsymbol{\theta}_i^T \mathbf{x})$, $i = 1, \dots, N$, learned *w.r.t* N different random seeds on \mathcal{P}_{in} , each with weights $\boldsymbol{\theta}_i \in \mathbb{R}^D$. The mode ensemble function is thus defined as

$g_{\text{ens}} : \mathbf{x} \rightarrow \text{sign}(\sum_{i=1}^N (\boldsymbol{\theta}_i^T \mathbf{x}))$. The following proposition states the superiority of mode ensemble in achieving a lower gap on the accuracy between InD data and OoD data over the average of multiple modes.

Proposition 1. Consider the in-distribution \mathcal{P}_{in} , out-distribution \mathcal{P}_{out} , and N independent modes $g_i, i = 1, \dots, N$ defined above, we have $\mathcal{G}(g_{\text{ens}}, \mathcal{P}_{\text{in}}, \mathcal{P}_{\text{out}}) \leq \frac{1}{N} \sum_{i=1}^N \mathcal{G}(g_i, \mathcal{P}_{\text{in}}, \mathcal{P}_{\text{out}})$, where

$$\mathcal{G}(g, \mathcal{P}_{\text{in}}, \mathcal{P}_{\text{out}}) = \left| \Phi^{-1}(\text{ACC}(g, \mathcal{P}_{\text{out}})) - \frac{\alpha}{\gamma} \Phi^{-1}(\text{ACC}(g, \mathcal{P}_{\text{in}})) \right| \quad (5)$$

denotes the gap of the probit-transformed accuracy between \mathcal{P}_{in} and \mathcal{P}_{out} achieved by the classifier g .

The proof of this proposition is deferred to the *supplementary material*. In the next section, extensive empirical results will verify the high variances on the OoD detection performance among independently trained models on InD data, and the substantial improvements brought by mode ensemble.

3 Empirical results

In experiments, we will empirically show (i) the high variances of independent modes on the OoD detection performance, (ii) the substantial improved detection results via mode ensemble in Sec.3.2 and Sec.3.3, respectively, and (iii) ablation studies on the independence of ensembled modes in Sec.3.4.

3.1 Setups

Following previous works on OoD detection [3, 4, 5, 6, 8, 9, 1, 10, 11, 12, 13], our experiments mainly cover both the small-scale CIFAR10 [28] and the large-scale ImageNet [29] data sets. For CIFAR10, 10 independently-trained models *w.r.t* 10 different random seeds are evaluated, including structures of ResNet18 [30] and Wide ResNet28x10 [31]. For ImageNet, 5 models of ResNet50 [30] and DenseNet121 [32] are independently trained *w.r.t* 5 different random seeds. We further train 3 independent models of T2T-ViT-14 [33] *w.r.t* 3 different random seeds from scratch on ImageNet to further evaluate the mode performance on such a transformer structure.

For CIFAR10 as the in-distribution, we evaluate the OoD detection performance of different modes on 5 out-distribution data sets: SVHN [34], LSUN [35], iSUN [36], Textures [37] and Places [38]. For ImageNet as the in-distribution, the selected OoD data sets include iNaturalist [39], SUN [40], Places [38] and Textures [37].

We select 7 representative and SOTA OoD detectors as the baselines, including MSP [3], ODIN [4], Energy [6], Mahalanobis [5], kNN [11], RankFeat [1] and GradNorm [9]. These are all post-hoc and OoD-agnostic detectors, covering logits-based (MSP, ODIN, Energy), features-based (Mahalanobis, kNN and RankFeat) and gradients-based (GradNorm) types. We evaluate the detection performance of these methods on multiple independent modes to show the high detection variances existing widely in different detector types and network structures, and then perform mode ensemble to reduce the variances and boost OoD detection performance. For each single and ensembling modes, we record their (i) InD classification accuracy, (ii) false positive rate (FPR) on OoD data sets when the true positive rate on InD data is 95% and (iii) area under the receiver operating characteristic curve (AUROC).

Remark For checkable reproducibility, all the training and evaluation code and the trained models are released¹ publicly. The details of model training and baseline detectors can be found in the *supplementary material*. Besides, for a clear elaboration, in the following 3 subsections, we mainly consider the 5 modes of DenseNet121 on ImageNet and the 6 common detectors, including 3 logits-based (MSP, ODIN and Energy), 1 gradients-based (GradNorm), and 2 features-based (Mahalanobis and RankFeat) detectors. Comprehensive results covering more modes on other InD and OoD datasets, baseline detectors and network structures are provided in the *supplementary material*.

mode	mode-1	mode-2	mode-3	mode-4	mode-5
InD Acc.	74.25	74.30	74.46	74.29	74.33

Table 1: The classification accuracy on the ImageNet validation set of 5 isolated modes of DenseNet121.

3.2 High variances among the independent modes for OoD detection

This subsection empirically presents the existence of a high variance in the OoD detection results of multiple isolated modes. The classification accuracy of these modes on the InD data is shown in Tab.1 to illustrate that these modes

¹<https://github.com/fanghenshaometeor/ood-mode-ensemble>

Modes	OoD data sets							
	iNaturalist		SUN		Places		Textures	
	FPR↓	AUROC↑	FPR↓	AUROC↑	FPR↓	AUROC↑	FPR↓	AUROC↑
MSP								
mode-1	58.44	87.18	71.11	80.78	74.11	79.69	67.07	80.72
mode-2	55.68	87.28	68.78	81.49	70.85	80.63	66.21	80.27
mode-3	58.29	87.10	70.60	81.02	73.01	80.07	66.06	80.70
mode-4	58.52	87.20	70.73	80.81	72.79	79.77	67.85	80.46
mode-5	60.97	86.19	70.82	80.69	72.76	79.89	64.41	80.93
ODIN								
mode-1	54.88	89.39	60.26	85.76	65.84	83.33	54.36	86.61
mode-2	50.56	90.21	55.79	87.00	60.81	85.08	53.35	86.62
mode-3	51.61	90.12	57.90	86.08	63.82	85.08	53.35	86.62
mode-4	51.47	90.26	59.03	86.28	63.56	84.01	55.12	86.20
mode-5	58.13	88.39	59.17	85.84	63.17	84.07	51.83	86.19
Energy								
mode-1	56.24	88.63	57.85	85.99	64.35	83.29	51.93	86.98
mode-2	52.86	89.67	53.31	87.32	59.77	85.16	50.76	87.05
mode-3	53.19	89.61	55.89	86.35	62.05	84.13	50.64	86.86
mode-4	53.31	89.77	56.85	86.58	62.75	84.08	53.56	86.53
mode-5	60.92	87.56	56.76	86.07	61.93	84.11	49.93	86.46
GradNorm								
mode-1	73.79	77.93	72.64	75.03	81.21	70.23	66.15	77.82
mode-2	69.99	79.89	68.30	76.72	75.71	72.63	63.30	78.74
mode-3	69.93	79.67	69.12	77.56	77.22	73.34	64.06	78.48
mode-4	66.85	81.07	72.51	75.61	80.08	71.44	65.87	77.27
mode-5	77.07	73.47	73.66	73.88	80.59	69.90	66.83	76.39
Mahalanobis								
mode-1	89.20	63.79	84.50	70.98	83.84	71.65	43.56	75.46
mode-2	93.31	60.90	85.98	68.14	83.87	71.11	65.21	58.26
mode-3	88.43	69.11	86.21	70.74	85.17	72.50	51.40	70.16
mode-4	91.84	58.88	86.82	66.23	85.54	69.64	49.86	68.64
mode-5	92.43	59.27	82.07	70.24	81.02	72.95	57.20	63.21
RankFeat								
mode-1	66.01	85.91	75.53	80.27	79.95	75.64	43.60	90.35
mode-2	58.49	83.77	34.70	92.02	50.70	86.12	32.73	92.45
mode-3	59.53	85.17	50.07	88.37	63.27	82.05	40.64	91.54
mode-4	84.70	78.61	69.57	83.82	76.45	78.21	49.89	90.81
mode-5	46.58	87.27	44.46	88.42	58.95	81.54	22.48	94.15

Table 2: The detection performance of each independent mode (DenseNet121 trained on ImageNet) on each OoD data set *w.r.t* different types of OoD detectors. The **best** and **worst** of the detection results among the 5 modes are highlighted.

are all well-trained on InD data. Then, regarding the OoD detection, the detection results of each mode *w.r.t* different detectors are reported in Tab.2.

In Tab.2, we mark the **best** and **worst** FPR and AUROC results of the 5 modes on each OoD data set achieved by different types of detectors. Though these modes all perform consistently well on the InD data in Tab.1, there clearly exists a large variance of the OoD detection results among independent modes for different detectors. Specifically, we can find the following two phenomena.

- For the same OoD detector, different modes hold significantly-fluctuating FPR results. For example, the RankFeat even reaches a worst FPR value 84.71% by the mode-4 and a best FPR value 46.58% by the mode-5 on the iNaturalist data set.

Ensemble of k modes	OoD data sets							
	iNaturalist		SUN		Places		Textures	
	FPR↓	AUROC↑	FPR↓	AUROC↑	FPR↓	AUROC↑	FPR↓	AUROC↑
	MSP							
$k = 1$	58.38±1.87	86.99±0.45	70.41±0.93	80.96±0.32	72.70±1.17	80.01±0.37	66.32±1.29	80.62±0.26
$k = 2$	54.69±1.01	88.29±0.24	68.75±0.39	82.03±0.04	70.72±0.37	81.21±0.12	64.05±0.57	81.58±0.05
$k = 3$	53.57±0.55	88.75±0.19	68.31±0.21	82.18±0.09	70.74±0.37	81.38±0.12	63.39±0.48	81.99±0.02
$k = 4$	53.42±0.49	88.94±0.11	68.48±0.15	82.34±0.01	70.47±0.35	81.52±0.06	63.35±0.78	82.11±0.07
	ODIN							
$k = 1$	53.33±3.14	89.67±0.80	58.43±1.70	86.19±0.50	63.44±1.80	84.31±0.76	53.51±1.28	86.43±0.22
$k = 2$	50.60±2.55	91.06±0.56	56.50±1.54	87.37±0.40	61.09±0.96	85.47±0.46	49.41±0.93	88.30±0.06
$k = 3$	48.43±0.89	91.76±0.15	55.75±0.35	87.62±0.11	60.59±0.49	85.78±0.16	47.49±0.22	88.86±0.14
$k = 4$	48.37±0.28	91.93±0.09	55.81±0.50	87.74±0.14	60.62±0.46	85.89±0.20	46.52±0.57	89.13±0.08
	Energy							
$k = 1$	55.30±3.42	89.05±0.95	56.13±1.72	86.46±0.53	62.17±1.65	84.15±0.66	51.36±1.42	86.78±0.27
$k = 2$	51.33±1.78	90.85±0.46	53.75±1.14	87.64±0.22	59.90±1.54	85.44±0.48	46.00±1.18	88.83±0.11
$k = 3$	49.58±1.60	91.52±0.28	52.72±1.04	88.05±0.20	58.84±1.19	85.93±0.33	44.27±0.51	89.48±0.03
$k = 4$	49.23±0.97	91.64±0.20	52.33±0.27	88.23±0.07	58.34±0.57	86.14±0.10	42.74±0.43	89.81±0.08
	GradNorm							
$k = 1$	71.53±3.96	78.41±2.98	71.25±2.38	75.76±1.44	78.96±2.38	71.51±1.49	65.24±1.49	77.74±0.95
$k = 2$	69.97±3.93	79.96±2.53	68.72±1.53	77.06±0.94	77.15±1.67	72.93±1.08	61.93±0.88	79.85±0.41
$k = 3$	67.58±2.53	81.99±1.44	67.78±0.41	77.97±0.32	76.43±0.49	73.69±0.27	60.71±0.75	81.05±0.19
$k = 4$	67.22±1.64	82.33±0.93	66.65±0.22	78.44±0.26	75.37±0.14	74.33±0.23	59.59±0.41	81.52±0.21
	Mahalanobis							
$k = 1$	91.04±2.12	62.39±4.22	85.12±1.90	69.27±2.03	83.89±1.77	71.57±1.30	53.45±8.17	67.15±6.61
$k = 2$	88.68±2.96	65.43±2.15	83.44±3.27	72.48±4.09	83.41±2.78	73.45±2.57	44.60±8.88	75.07±5.99
$k = 3$	83.25±6.50	72.39±3.72	82.77±5.00	76.03±4.03	83.83±3.40	74.50±2.54	37.22±7.31	82.91±4.23
$k = 4$	81.49±2.78	72.42±2.48	82.59±4.45	76.15±3.11	84.14±3.55	74.44±2.07	39.01±7.63	81.81±5.44
	RankFeat							
$k = 1$	63.06±13.98	84.15±3.34	54.87±17.18	86.58±4.57	65.86±12.20	80.71±3.99	37.87±10.59	91.86±1.51
$k = 2$	49.18±13.04	89.67±2.61	45.30±11.30	89.80±2.57	59.64±8.77	83.70±2.61	23.21±2.71	95.04±0.10
$k = 3$	45.78±10.18	90.96±1.93	43.45±3.39	90.57±0.82	58.07±2.18	84.49±0.69	18.98±0.51	95.98±0.25
$k = 4$	40.92±5.41	91.82±0.99	38.68±3.01	91.51±0.52	54.84±2.31	85.38±0.49	16.44±0.77	96.43±0.36

Table 3: The detection performance of ensembling k independent modes (DenseNet121 trained on ImageNet) on each OoD data set *w.r.t* different types of OoD detectors. Results with the **lowest variances** are highlighted with bold fonts.

- For different modes, detection results among those methods might be opposite. For example, considering the mode-4, Energy achieves better detection result on iNaturalist (53.31%) than RankFeat (84.70%), while for the mode-5, RankFeat (46.58%) outperforms Energy (60.92%) a lot.

Such widely-existed high variances support our viewpoint: *The OoD detection performance of single modes is of high uncertainty*. In addition, these phenomena are more conspicuous on the small-scale CIFAR10 data set with even higher variances of the detection FPR results among independent modes, see the *supplementary material* for complete results and more analysis.

3.3 Mode ensemble stabilizes and boosts OoD detection

In this subsection, mode ensemble is introduced to alleviate the high variances of the OoD detection performance among multiple isolated modes and to further boost the detection. Tab.3 shows the OoD detection performance of ensembling k modes. For $k = 1$, we record the mean values and standard deviations of the detection results among the total N modes. For each $k > 1$, firstly k different modes are randomly selected and get ensemble to perform OoD detection, then such process is repeated 3 times to calculate the mean values and standard deviations of the detection results of ensembling k modes.

As shown in Tab.3, regarding the aforementioned 2 phenomena in the preceding subsection, we can find:

- For the same OoD detector, mode ensemble could significantly reduce the detection variances and substantially improve the detection performance. For example, the mean FPR results of RankFeat on iNaturalist get improved from 63.06% to 40.92% with a variance reduction from 13.98 to 5.41.

- Such rather stable detection results brought by mode ensemble also benefit the evaluation of those OoD detectors and get rid of the uncertainties of single modes.

The advantages of mode ensemble, *i.e.*, variance reduction and performance improvements, are also widely reflected on the small-scale data set CIFAR10 and more network structures (residual networks and vision transformers) for different types of OoD detectors. Refer to the *supplementary material* for thorough results on mode ensemble for OoD detection.

3.4 Ablation studies

In this section, ablation studies are executed to show that the ensemble of those modes, which are from the same trajectory and are not independent, can not bring OoD detection performance improvements.

Given a well-trained mode f_{s_n} with parameters $\omega_{s_n} \in \mathbb{R}^K$ *w.r.t* a random seed s_n , we obtain M modes $f_{s_n}^{(i)}, i = 1, \dots, M$ by sampling from the subspace of f_{s_n} as follows:

$$\omega_{s_n}^{(i)} = \omega_{s_n} + r \cdot \frac{\mathbf{u}}{\|\mathbf{u}\|}, i = 1, \dots, M, \quad (6)$$

where $\mathbf{u} \in \mathcal{N}(0^K, 1^K)$ and r denotes a random step size. In this way, the obtained M modes $f_{s_n}^{(i)}$ are not independent with each other and are concentrated around f_{s_n} . Comparison results between ensembling such modes and ensembling the independent modes on InD recognition accuracy and OoD detection FPR values are shown in Fig.5.

As shown in Fig.5, on the one hand, mode ensemble could bring higher InD accuracy and lower OoD FPR values for both the 2 types of modes that are isolated with each other or are all sampled from the same subspace. On the other hand, ensembling those independent modes clearly shows better generalization performance on InD data and stronger detection performance on OoD data than ensembling those modes that are not isolated. From the perspective of loss landscape, those isolated modes *w.r.t* different trajectories hold much more diversified information than those modes concentrated around the same trajectory, thereby leading to better ensemble performance in both InD generalization and OoD detection.

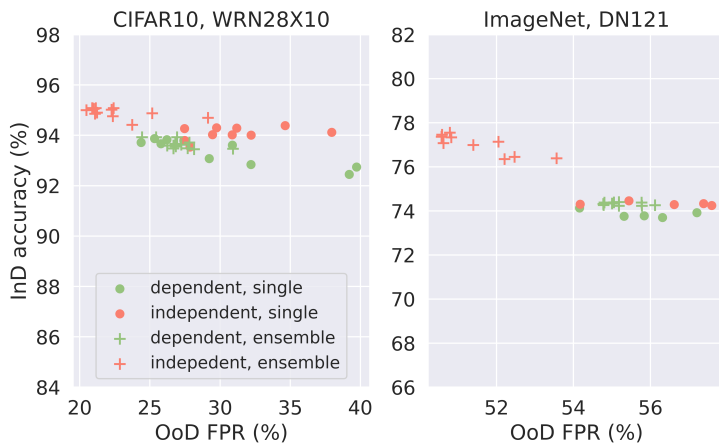


Figure 5: Ablation studies on the independence of modes. Each data point indicates the results of one single mode (circle dots) or ensembled modes (plus markers) with InD accuracy (y-axis) and average detection FPR over multiple OoD data sets (x-axis) achieved by Energy.

4 Related work

4.1 OoD detection

The task of OoD detection focuses on the detection ability of DNNs on data from an out-distribution differing from the training distribution [41]. Plenty of researches have been developed from various aspects, see reviews in [14, 15].

Aside from the outlined 3 types of detectors, logits-based, features-based and gradients-based, in Sec.1, which are mainly post-hoc and OoD-agnostic, there exist other detectors that work on the training process via additional data or

model modifications. For example, G-ODIN [42] designs a two-branch network architecture to decompose the output probabilities and to alleviate the over-confidence on OoD data. An autoencoder is introduced for OoD detection in an unsupervised way with the Stiefel-Restricted Kernel Machine in [43]. [44] discusses 2 different distribution shifts for the out-distribution and proposes semantics information as the detection metric.

Related theoretical works in OoD detection mainly study single modes. A theoretical framework for OoD generalization is formalized in [45]. The probably approximated correct learning theory for OoD detection is investigated in [46]. Our theoretical work discusses mode ensemble for OoD detection in a simple binary classification problem on Gaussian distributions.

4.2 Mode, loss landscape and ensemble

Mode and loss landscape Analyzing the mode properties in the loss landscape of DNNs could date back to [47], which shows that the loss along a straight line connecting the initialization and the final solution monotonically decreases. Then, [17] and [16] find low-loss curves that connect two independent modes in the loss landscape and [19] proposes a training algorithm to learn subspaces of DNNs in the forms of lines, Bezier curves and simplexes. Mode connectivity has also inspired researches in other fields. For example, [48, 49] leverage mode connectivity for more robust neural networks against adversarial examples. [50] proposes weight-averaging on the independent modes for better OoD generalization.

Ensemble Ensemble has been a useful technique to improve the model generalization performance on the InD test data in both traditional machine learning [51] and the deep learning [20]. [18] visualizes and quantitatively measures the functional space diversity in the loss landscape to show how deep ensemble boosts the generalization performance on InD data. Besides, the ensemble technique has been widely utilized in different fields, such as adversarial and certified robustness [52, 53, 54] and machinery fault diagnosis [55].

5 Conclusion and discussion

In this work, starting from the loss landscape perspective, we observe that those independent modes, which are trained to achieve low-loss regions on InD data, yet yield significantly different loss landscapes of OoD data. The research community has ignored the uncertainties brought by such diversities across single modes on the OoD loss landscape: (i) For the same OoD detector, independent modes could hold substantially varied detection performance, and (ii) For two OoD detectors, different modes could yield opposite performance. Accordingly, to alleviate the high variances, we revisit the deep ensemble method to ensemble multiple independent modes so as to achieve stable results and substantially improve detecting OoD data, which also benefits the development and evaluation on OoD detectors in the sense of reduced variances. Our experiments cover different types of OoD detectors, various network structures, small-scale and large-scale data sets and ablation studies on the independence of modes, supporting our viewpoint comprehensively and solidly together with the theoretical analysis on the reduced accuracy gap between InD and OoD data brought by ensemble.

On the other hand, there inevitably exist limitations of the mode ensemble for OoD detection. Obtaining multiple isolated modes requires independently training multiple DNNs, which is time-consuming and memory-inefficient. Nevertheless, we hope that our work could bring the community with new ideas of investigating the OoD detection across independent modes from the loss landscape perspective. Future works will be devoted to deeply exploring the mode properties connecting the OoD data with the InD data.

References

- [1] Yue Song, Nicu Sebe, and Wei Wang. Rankfeat: Rank-1 feature removal for out-of-distribution detection. *Advances in Neural Information Processing Systems*, 35:17885–17898, 2022.
- [2] Chiyuan Zhang, Samy Bengio, Moritz Hardt, Benjamin Recht, and Oriol Vinyals. Understanding deep learning (still) requires rethinking generalization. *Communications of the ACM*, 64(3):107–115, 2021.
- [3] Dan Hendrycks and Kevin Gimpel. A baseline for detecting misclassified and out-of-distribution examples in neural networks. In *International Conference on Learning Representations*, 2016.
- [4] Shiyu Liang, Yixuan Li, and R Srikant. Enhancing the reliability of out-of-distribution image detection in neural networks. In *International Conference on Learning Representations*, 2018.
- [5] Kimin Lee, Kibok Lee, Honglak Lee, and Jinwoo Shin. A simple unified framework for detecting out-of-distribution samples and adversarial attacks. *Advances in neural information processing systems*, 31, 2018.

- [6] Weitang Liu, Xiaoyun Wang, John Owens, and Yixuan Li. Energy-based out-of-distribution detection. Advances in neural information processing systems, 33:21464–21475, 2020.
- [7] Jinsol Lee and Ghassan AlRegib. Gradients as a measure of uncertainty in neural networks. In 2020 IEEE International Conference on Image Processing (ICIP), pages 2416–2420. IEEE, 2020.
- [8] Yiyu Sun, Chuan Guo, and Yixuan Li. React: Out-of-distribution detection with rectified activations. Advances in Neural Information Processing Systems, 34:144–157, 2021.
- [9] Rui Huang, Andrew Geng, and Yixuan Li. On the importance of gradients for detecting distributional shifts in the wild. Advances in Neural Information Processing Systems, 34:677–689, 2021.
- [10] Yao Zhu, YueFeng Chen, Chuanlong Xie, Xiaodan Li, Rong Zhang, Hui Xue, Xiang Tian, Yaowu Chen, et al. Boosting out-of-distribution detection with typical features. Advances in Neural Information Processing Systems, 35:20758–20769, 2022.
- [11] Yiyu Sun, Yifei Ming, Xiaojin Zhu, and Yixuan Li. Out-of-distribution detection with deep nearest neighbors. In International Conference on Machine Learning, pages 20827–20840. PMLR, 2022.
- [12] Haoqi Wang, Zhizhong Li, Litong Feng, and Wayne Zhang. Vim: Out-of-distribution with virtual-logit matching. In Proceedings of the IEEE/CVF Conference on Computer Vision and Pattern Recognition, pages 4921–4930, 2022.
- [13] Yeonguk Yu, Sungho Shin, Seongju Lee, Changhyun Jun, and Kyoobin Lee. Block selection method for using feature norm in out-of-distribution detection. In Proceedings of the IEEE/CVF Conference on Computer Vision and Pattern Recognition, pages 15701–15711, 2023.
- [14] Jinggang Yang, Kaiyang Zhou, Yixuan Li, and Ziwei Liu. Generalized out-of-distribution detection: A survey. arXiv preprint arXiv:2110.11334, 2021.
- [15] Zheyang Shen, Jiashuo Liu, Yue He, Xingxuan Zhang, Renzhe Xu, Han Yu, and Peng Cui. Towards out-of-distribution generalization: A survey. arXiv preprint arXiv:2108.13624, 2021.
- [16] Timur Garipov, Pavel Izmailov, Dmitrii Podoprikin, Dmitry P Vetrov, and Andrew G Wilson. Loss surfaces, mode connectivity, and fast ensembling of dnns. Advances in neural information processing systems, 31, 2018.
- [17] Felix Draxler, Kambis Veschgini, Manfred Salmhofer, and Fred Hamprecht. Essentially no barriers in neural network energy landscape. In International conference on machine learning, pages 1309–1318. PMLR, 2018.
- [18] Stanislav Fort, Huiyi Hu, and Balaji Lakshminarayanan. Deep ensembles: A loss landscape perspective. arXiv preprint arXiv:1912.02757, 2019.
- [19] Mitchell Wortsman, Maxwell C Horton, Carlos Guestrin, Ali Farhadi, and Mohammad Rastegari. Learning neural network subspaces. In International Conference on Machine Learning, pages 11217–11227. PMLR, 2021.
- [20] Balaji Lakshminarayanan, Alexander Pritzel, and Charles Blundell. Simple and scalable predictive uncertainty estimation using deep ensembles. Advances in neural information processing systems, 30, 2017.
- [21] Alexey Dosovitskiy, Lucas Beyer, Alexander Kolesnikov, Dirk Weissenborn, Xiaohua Zhai, Thomas Unterthiner, Mostafa Dehghani, Matthias Minderer, Georg Heigold, Sylvain Gelly, et al. An image is worth 16x16 words: Transformers for image recognition at scale. In International Conference on Learning Representations, 2020.
- [22] Laurens Van der Maaten and Geoffrey Hinton. Visualizing data using t-sne. Journal of machine learning research, 9(11), 2008.
- [23] Hao Li, Zheng Xu, Gavin Taylor, Christoph Studer, and Tom Goldstein. Visualizing the loss landscape of neural nets. Advances in neural information processing systems, 31, 2018.
- [24] Feng Xue, Zi He, Chuanlong Xie, Falong Tan, and Zhenguo Li. Boosting out-of-distribution detection with multiple pre-trained models. arXiv preprint arXiv:2212.12720, 2022.
- [25] Apoorv Vyas, Nataraj Jammalamadaka, Xia Zhu, Dipankar Das, Bharat Kaul, and Theodore L Willke. Out-of-distribution detection using an ensemble of self supervised leave-out classifiers. In Proceedings of the European Conference on Computer Vision (ECCV), pages 550–564, 2018.
- [26] Donghun Yang, Kien Mai Ngoc, Iksoo Shin, Kyong-Ha Lee, and Myungwon Hwang. Ensemble-based out-of-distribution detection. Electronics, 10(5):567, 2021.
- [27] John P Miller, Rohan Taori, Aditi Raghunathan, Shiori Sagawa, Pang Wei Koh, Vaishaal Shankar, Percy Liang, Yair Carmon, and Ludwig Schmidt. Accuracy on the line: on the strong correlation between out-of-distribution and in-distribution generalization. In International Conference on Machine Learning, pages 7721–7735. PMLR, 2021.

- [28] A Krizhevsky. Learning multiple layers of features from tiny images. Master’s thesis, University of Toronto, 2009.
- [29] Jia Deng, Wei Dong, Richard Socher, Li-Jia Li, Kai Li, and Li Fei-Fei. Imagenet: A large-scale hierarchical image database. In IEEE Conference on Computer Vision and Pattern Recognition, pages 248–255, 2009.
- [30] Kaiming He, Xiangyu Zhang, Shaoqing Ren, and Jian Sun. Deep residual learning for image recognition. In IEEE Conference on Computer Vision and Pattern Recognition, pages 770–778, 2016.
- [31] Sergey Zagoruyko and Nikos Komodakis. Wide residual networks. In British Machine Vision Conference 2016. British Machine Vision Association, 2016.
- [32] Gao Huang, Zhuang Liu, Laurens Van Der Maaten, and Kilian Q Weinberger. Densely connected convolutional networks. In Proceedings of the IEEE conference on computer vision and pattern recognition, pages 4700–4708, 2017.
- [33] Li Yuan, Yunpeng Chen, Tao Wang, Weihao Yu, Yujun Shi, Zi-Hang Jiang, Francis EH Tay, Jiashi Feng, and Shuicheng Yan. Tokens-to-token vit: Training vision transformers from scratch on imagenet. In Proceedings of the IEEE/CVF international conference on computer vision, pages 558–567, 2021.
- [34] Yuval Netzer, Tao Wang, Adam Coates, Alessandro Bissacco, Bo Wu, and Andrew Y Ng. Reading digits in natural images with unsupervised feature learning. In Proceedings of the NIPS Workshop on Deep Learning and Unsupervised Feature Learning, 2011.
- [35] Fisher Yu, Ari Seff, Yinda Zhang, Shuran Song, Thomas Funkhouser, and Jianxiong Xiao. Lsun: Construction of a large-scale image dataset using deep learning with humans in the loop. arXiv preprint arXiv:1506.03365, 2015.
- [36] Pingmei Xu, Krista A Ehinger, Yinda Zhang, Adam Finkelstein, Sanjeev R Kulkarni, and Jianxiong Xiao. Turkergaze: Crowdsourcing saliency with webcam based eye tracking. arXiv preprint arXiv:1504.06755, 2015.
- [37] Mircea Cimpoi, Subhansu Maji, Iasonas Kokkinos, Sammy Mohamed, and Andrea Vedaldi. Describing textures in the wild. In Proceedings of the IEEE conference on computer vision and pattern recognition, pages 3606–3613, 2014.
- [38] Bolei Zhou, Agata Lapedriza, Aditya Khosla, Aude Oliva, and Antonio Torralba. Places: A 10 million image database for scene recognition. IEEE transactions on pattern analysis and machine intelligence, 40(6):1452–1464, 2017.
- [39] Grant Van Horn, Oisin Mac Aodha, Yang Song, Yin Cui, Chen Sun, Alex Shepard, Hartwig Adam, Pietro Perona, and Serge Belongie. The inaturalist species classification and detection dataset. In Proceedings of the IEEE conference on computer vision and pattern recognition, pages 8769–8778, 2018.
- [40] Jianxiong Xiao, James Hays, Krista A Ehinger, Aude Oliva, and Antonio Torralba. Sun database: Large-scale scene recognition from abbey to zoo. In 2010 IEEE computer society conference on computer vision and pattern recognition, pages 3485–3492. IEEE, 2010.
- [41] Anh Nguyen, Jason Yosinski, and Jeff Clune. Deep neural networks are easily fooled: High confidence predictions for unrecognizable images. In Proceedings of the IEEE conference on computer vision and pattern recognition, pages 427–436, 2015.
- [42] Yen-Chang Hsu, Yilin Shen, Hongxia Jin, and Zsolt Kira. Generalized odin: Detecting out-of-distribution image without learning from out-of-distribution data. In Proceedings of the IEEE/CVF Conference on Computer Vision and Pattern Recognition, pages 10951–10960, 2020.
- [43] Francesco Tonin, Arun Pandey, Panagiotis Patrinos, and Johan AK Suykens. Unsupervised energy-based out-of-distribution detection using stiefel-restricted kernel machine. In 2021 International Joint Conference on Neural Networks (IJCNN), pages 1–8. IEEE, 2021.
- [44] Jingkang Yang, Kaiyang Zhou, and Ziwei Liu. Full-spectrum out-of-distribution detection. International Journal of Computer Vision, pages 1–16, 2023.
- [45] Haotian Ye, Chuanlong Xie, Tianle Cai, Ruichen Li, Zhenguo Li, and Liwei Wang. Towards a theoretical framework of out-of-distribution generalization. Advances in Neural Information Processing Systems, 34:23519–23531, 2021.
- [46] Zhen Fang, Yixuan Li, Jie Lu, Jiahua Dong, Bo Han, and Feng Liu. Is out-of-distribution detection learnable? Advances in Neural Information Processing Systems, 35:37199–37213, 2022.
- [47] Ian J Goodfellow, Oriol Vinyals, and Andrew M Saxe. Qualitatively characterizing neural network optimization problems. In International Conference on Learning Representations, 2015.
- [48] Pu Zhao, Pin-Yu Chen, Payel Das, Karthikeyan Natesan Ramamurthy, and Xue Lin. Bridging mode connectivity in loss landscapes and adversarial robustness. In International Conference on Learning Representations, 2020.

- [49] Ren Wang, Yuxuan Li, and Sijia Liu. Exploring diversified adversarial robustness in neural networks via robust mode connectivity. In Proceedings of the IEEE/CVF Conference on Computer Vision and Pattern Recognition, pages 2345–2351, 2023.
- [50] Alexandre Rame, Matthieu Kirchmeyer, Thibaud Rahier, Alain Rakotomamonjy, Patrick Gallinari, and Matthieu Cord. Diverse weight averaging for out-of-distribution generalization. Advances in Neural Information Processing Systems, 35:10821–10836, 2022.
- [51] Zhi-Hua Zhou. Ensemble methods: foundations and algorithms. CRC press, 2012.
- [52] Kun Fang, Qinghua Tao, Yingwen Wu, Tao Li, Jia Cai, Feipeng Cai, Xiaolin Huang, and Jie Yang. Towards robust neural networks via orthogonal diversity. arXiv preprint arXiv:2010.12190, 2020.
- [53] Miklós Z Horváth, Mark Niklas Mueller, Marc Fischer, and Martin Vechev. Boosting randomized smoothing with variance reduced classifiers. In International Conference on Learning Representations, 2021.
- [54] Kun Fang, Qinghua Tao, Yingwen Wu, Tao Li, Xiaolin Huang, and Jie Yang. On multi-head ensemble of smoothed classifiers for certified robustness. arXiv preprint arXiv:2211.10882, 2022.
- [55] Te Han and Yan-Fu Li. Out-of-distribution detection-assisted trustworthy machinery fault diagnosis approach with uncertainty-aware deep ensembles. Reliability Engineering & System Safety, 226:108648, 2022.

Supplementary Material for Revisiting Deep Ensemble for Out-of-Distribution Detection: A Loss Landscape Perspective

I Baseline OoD detectors and the corresponding mode ensemble

We outline how the scoring function $S(\cdot)$ is designed in the selected baseline OoD detectors and elaborate the corresponding mode ensemble strategies over these detectors. In the following, the outputs of the mode $f : \mathbb{R}^D \rightarrow \mathbb{R}^C$ are the logits of C -dimension, in correspondence to C classes.

MSP [3] takes the maximum probability over the output logits as the scoring function. Given a test sample $\mathbf{x} \in \mathbb{R}^D$, its MSP score *w.r.t* a single mode $f(\cdot)$ is

$$S_{\text{MSP}}(\mathbf{x}) = \max(\text{softmax}(f(\mathbf{x}))). \quad (\text{I.1})$$

MSP-ensemble adopts the maximum probability over the average logits from N modes $f_{s_i}, i = 1, \dots, N$ as the score for \mathbf{x} :

$$S_{\text{MSP-ens}}(\mathbf{x}) = \max\left(\text{softmax}\left(\frac{1}{N} \sum_{i=1}^N f_{s_i}(\mathbf{x})\right)\right). \quad (\text{I.2})$$

ODIN [4] introduces temperature scaling and adversarial examples into MSP and proposes the following score:

$$S_{\text{ODIN}}(\mathbf{x}) = \max\left(\text{softmax}\left(\frac{f(\bar{\mathbf{x}})}{T}\right)\right), \quad (\text{I.3})$$

where T denotes the temperature and $\bar{\mathbf{x}}$ denotes the perturbed adversarial examples. Following the settings in [4, 1], we set $T = 1000$ and do not perturb \mathbf{x} for ImageNet in experiments.

ODIN-ensemble shares a similar scoring function with MSP-ensemble:

$$S_{\text{ODIN-ens}}(\mathbf{x}) = \max\left(\text{softmax}\left(\frac{\sum_{i=1}^N f_{s_i}(\bar{\mathbf{x}})}{N \cdot T}\right)\right). \quad (\text{I.4})$$

The adversarial attack is executed individually on each mode f_{s_i} and then the ODIN score is calculated on the average predictive logits on the perturbed inputs.

Energy [6] improves MSP via an energy function since energy is better aligned with the input probability density:

$$S_{\text{energy}}(\mathbf{x}) = \log \sum_{i=1}^C \exp(f^i(\mathbf{x})), \quad (\text{I.5})$$

where $f^i(\mathbf{x})$ denotes the i -th element in the C -dimension output logits.

Energy-ensemble firstly averages the N logits and then computes the energy score:

$$S_{\text{energy-ens}}(\mathbf{x}) = \log \sum_{i=1}^C \exp(f_{\text{ens}}^i(\mathbf{x})), \quad f_{\text{ens}}(\mathbf{x}) = \frac{1}{N} \sum_{i=1}^N f_{s_i}(\mathbf{x}). \quad (\text{I.6})$$

Mahalanobis [5] tries to model the network outputs at different layers as the mixture of multivariate Gaussian distributions and uses the Mahalanobis distance as the scoring function:

$$S_{\text{mahal}}(\mathbf{x}) = \max_c \left(-(f(\mathbf{x}) - \boldsymbol{\mu}_c)^T \Sigma (f(\mathbf{x}) - \boldsymbol{\mu}_c) \right), \quad (\text{I.7})$$

where $\boldsymbol{\mu}_c$ denotes the mean feature vector of class- c and Σ denotes the covariance matrix across classes. In experiments, following the settings in [5, 1], adversarial examples generated from 500 randomly-selected clean samples are involved to train the logistic regression, with a perturbation size 0.05 on CIFAR10 and 0.001 on ImageNet.

Mahalanobis-ensemble mainly leverages the average output features at the same layers in DNNs over N modes and attacks the N modes simultaneously to calculate the Mahalanobis score. Details can be found in the released code.

kNN [11] is a simple but time-consuming and memory-inefficient detector since it performs nearest neighbor search on the ℓ_2 -normalized penultimate features between the test sample and all the training samples. The negative of the (k -th) shortest ℓ_2 distance between the test features and all the training features is set as the score for a new sample \mathbf{x}^* :

$$S_{\text{knn}}(\mathbf{x}^*) = - \min_{i:1, \dots, n_{\text{tr}}} \left\| \frac{\mathbf{h}^*}{\|\mathbf{h}^*\|_2} - \frac{\mathbf{h}^i}{\|\mathbf{h}^i\|_2} \right\|_2, \quad (\text{I.8})$$

where \mathbf{h} denotes the penultimate features in the DNN, and \mathbf{h}^i denotes the penultimate features in correspondence to the i -th training sample in the training set of size n_{tr} . The key of this detector is the ℓ_2 normalization on the features.

kNN-ensemble improves performance by replacing the penultimate features from one single mode with the average penultimate features from N nodes:

$$S_{\text{knn-ens}}(\mathbf{x}^*) = - \min_{j:1, \dots, n_{\text{tr}}} \left\| \frac{\sum_{i=1}^N \mathbf{h}_{s_i}^*}{\|\sum_{i=1}^N \mathbf{h}_{s_i}^*\|_2} - \frac{\sum_{i=1}^N \mathbf{h}_{s_i}^j}{\|\sum_{i=1}^N \mathbf{h}_{s_i}^j\|_2} \right\|_2. \quad (\text{I.9})$$

RankFeat [1] removes the rank-1 matrix from each individual sample feature matrix \mathbf{X} in the mini-batch during forward propagation in test, since the rank-1 feature drastically perturbs the predictions on OoD samples:

$$\begin{aligned} \mathbf{X} &= \mathbf{U}\mathbf{S}\mathbf{V}^T, \\ \mathbf{X}' &= \mathbf{X} - s_1 \mathbf{u}_1 \mathbf{v}_1^T. \end{aligned} \quad (\text{I.10})$$

In Eq.(I.10), the singular value decomposition is firstly executed on the feature matrix \mathbf{X} of an individual sample, leading to the left and right orthogonal singular vector matrices \mathbf{U} and \mathbf{V} , and the rectangle diagonal singular value matrix \mathbf{S} . Then, the rank-1 matrix is calculated based on the largest singular value s_1 and the two corresponding singular vectors \mathbf{u}_1 and \mathbf{v}_1 , and gets subtracted from the original \mathbf{X} . Such removals are recommended at the 3rd and 4th blocks in DNNs. Finally, an Energy score is calculated on the resulting changed output logits.

RankFeat-ensemble executes the rank-1 feature removing on each mode individually and then average the N changed logits to compute the Energy score as Eq.(I.6). Details can be found in the released code.

GradNorm [9] leverages the gradient information for OoD detection by calculating the ℓ_1 norm of the gradients *w.r.t* a KL divergence loss as the score of \mathbf{x} :

$$S_{\text{GradNorm}}(\mathbf{x}) = \left\| \frac{\partial \text{KL}(\mathbf{u} \parallel \text{softmax}(f(\mathbf{x})))}{\partial \boldsymbol{\omega}} \right\|_1, \quad (\text{I.11})$$

where $\mathbf{u} = [1/C, \dots, 1/C] \in \mathbb{R}^C$ and $\boldsymbol{\omega}$ is recommended as the weight parameters of the last full-connected layer in DNNs.

GradNorm-ensemble firstly calculates the KL divergence between \mathbf{u} and the softmax probability of the average logits of N modes. The final score for \mathbf{x} is the average gradient norm over the selected parameters $\boldsymbol{\omega}_{s_i}$ in each mode:

$$S_{\text{GradNorm-ens}}(\mathbf{x}) = \frac{1}{N} \sum_{i=1}^N \left\| \frac{\partial \text{KL}(\mathbf{u} \parallel \text{softmax}(f_{\text{ens}}(\mathbf{x})))}{\partial \boldsymbol{\omega}_{s_i}} \right\|_1, \quad f_{\text{ens}}(\mathbf{x}) = \frac{1}{N} \sum_{i=1}^N f_{s_i}(\mathbf{x}). \quad (\text{I.12})$$

II Theoretical analysis

This section gives the proof of Proposition 1 in the manuscript, which is reiterated as follows.

Proposition 1'. Consider the in-distribution \mathcal{P}_{in} and the out-distribution \mathcal{P}_{out} , and the N modes $g_i, i = 1, \dots, N$, we have $\mathcal{G}(g_{\text{ens}}, \mathcal{P}_{\text{in}}, \mathcal{P}_{\text{out}}) \leq \frac{1}{N} \sum_{i=1}^N \mathcal{G}(g_i, \mathcal{P}_{\text{in}}, \mathcal{P}_{\text{out}})$, where

$$\mathcal{G}(g, \mathcal{P}_{\text{in}}, \mathcal{P}_{\text{out}}) = \left| \Phi^{-1}(\text{ACC}(g, \mathcal{P}_{\text{out}})) - \frac{\alpha}{\gamma} \Phi^{-1}(\text{ACC}(g, \mathcal{P}_{\text{in}})) \right| \quad (\text{II.1})$$

denotes the gap of the probit-transformed accuracy between \mathcal{P}_{in} and \mathcal{P}_{out} achieved by the classifier g .

Proof. Given the in-distribution \mathcal{P}_{in} defined as a Gaussian distribution $\mathcal{P}_{\text{in}} = \{(\mathbf{x}, y) \mid \mathbf{x} \sim \mathcal{N}(\boldsymbol{\mu} \cdot y; \sigma^2 I_{D \times D})\}$ with $\mathbf{x} \in \mathbb{R}^D$ and $y \in \{-1, 1\}$, and one single mode in the form of a linear classifier $g_i : \mathbf{x} \rightarrow \text{sign}(\boldsymbol{\theta}_i^T \mathbf{x}), i = 1, \dots, N$,

we have

$$\begin{aligned} ACC(g_i, \mathcal{P}_{in}) &= \Pr(\text{sign}(\boldsymbol{\theta}_i^T \mathbf{x}) = y) = \Pr(y \cdot (\boldsymbol{\theta}_i^T \mathbf{x}) > 0) \\ &= \Pr(\mathcal{N}(\boldsymbol{\theta}_i^T \boldsymbol{\mu}; \|\boldsymbol{\theta}_i\|^2 \sigma^2) \geq 0) = \Pr(\|\boldsymbol{\theta}_i\| \sigma \cdot \mathcal{N}(0; 1) \geq -(\boldsymbol{\theta}_i^T \boldsymbol{\mu})) = \Phi\left(\frac{\boldsymbol{\theta}_i^T \boldsymbol{\mu}}{\|\boldsymbol{\theta}_i\| \sigma}\right). \end{aligned} \quad (\text{II.2})$$

Similarly, for the out-distribution \mathcal{P}_{out} defined as a shift from \mathcal{P}_{in} : $\mathcal{P}_{out} = \{(\mathbf{x}, y) \mid \mathbf{x} \sim \mathcal{N}(\boldsymbol{\mu}' \cdot y; \sigma'^2 I_{D \times D})\}$ with $\boldsymbol{\mu}' = \alpha \cdot \boldsymbol{\mu} + \beta \cdot \boldsymbol{\Delta}$ and $\sigma' = \gamma \cdot \sigma$, and the mode ensemble function $g_{ens} : \mathbf{x} \rightarrow \text{sign}(\sum_{i=1}^N (\boldsymbol{\theta}_i^T \mathbf{x}))$, we have

$$\begin{aligned} ACC(g_i, \mathcal{P}_{out}) &= \Phi\left(\frac{\boldsymbol{\theta}_i^T \boldsymbol{\mu}'}{\|\boldsymbol{\theta}_i\| \sigma'}\right) = \Phi\left(\frac{\alpha}{\gamma} \cdot \frac{\boldsymbol{\theta}_i^T \boldsymbol{\mu}}{\|\boldsymbol{\theta}_i\| \sigma} + \frac{\beta}{\gamma \sigma} \cdot \frac{\boldsymbol{\theta}_i^T \boldsymbol{\Delta}}{\|\boldsymbol{\theta}_i\|}\right), \\ ACC(g_{ens}, \mathcal{P}_{in}) &= \Phi\left(\frac{\sum_{i=1}^N (\boldsymbol{\theta}_i^T \boldsymbol{\mu})}{\|\sum_{i=1}^N \boldsymbol{\theta}_i\| \sigma}\right), \\ ACC(g_{ens}, \mathcal{P}_{out}) &= \Phi\left(\frac{\alpha}{\gamma} \cdot \frac{\sum_{i=1}^N (\boldsymbol{\theta}_i^T \boldsymbol{\mu})}{\|\sum_{i=1}^N \boldsymbol{\theta}_i\| \sigma} + \frac{\beta}{\gamma \sigma} \cdot \frac{\sum_{i=1}^N (\boldsymbol{\theta}_i^T \boldsymbol{\Delta})}{\|\sum_{i=1}^N \boldsymbol{\theta}_i\|}\right). \end{aligned} \quad (\text{II.3})$$

Substituting Eq.(II.2) and Eq.(II.3) into Eq.(II.1), we have

$$\begin{aligned} \mathcal{G}_{avg} &\triangleq \frac{1}{N} \sum_{i=1}^N \mathcal{G}(g_i, \mathcal{P}_{in}, \mathcal{P}_{out}) = \frac{\beta}{\gamma \sigma} \cdot \frac{1}{N} \sum_{i=1}^N \frac{|\boldsymbol{\theta}_i^T \boldsymbol{\Delta}|}{\|\boldsymbol{\theta}_i\|}, \\ \mathcal{G}_{ens} &\triangleq \mathcal{G}(g_{ens}, \mathcal{P}_{in}, \mathcal{P}_{out}) = \frac{\beta}{\gamma \sigma} \cdot \frac{|\sum_{i=1}^N (\boldsymbol{\theta}_i^T \boldsymbol{\Delta})|}{\|\sum_{i=1}^N \boldsymbol{\theta}_i\|}. \end{aligned} \quad (\text{II.4})$$

If we are able to show that $\mathcal{G}_{ens} \leq \mathcal{G}_{avg}$ then the proof is finished. The derivations continue as follows.

$$\begin{aligned} \mathcal{G}_{avg} &= \frac{\beta}{\gamma \sigma} \cdot \frac{1}{N} \sum_{i=1}^N \frac{\|\boldsymbol{\theta}_i\| \|\boldsymbol{\Delta}\| |\cos\langle \boldsymbol{\theta}_i, \boldsymbol{\Delta} \rangle|}{\|\boldsymbol{\theta}_i\|} = \frac{\beta}{\gamma \sigma} \cdot \|\boldsymbol{\Delta}\| \frac{|\cos\langle \boldsymbol{\theta}_1, \boldsymbol{\Delta} \rangle| + \dots + |\cos\langle \boldsymbol{\theta}_N, \boldsymbol{\Delta} \rangle|}{N}, \\ \mathcal{G}_{ens} &= \frac{\beta}{\gamma \sigma} \cdot \frac{|\sum_{i=1}^N (\|\boldsymbol{\theta}_i\| \|\boldsymbol{\Delta}\| \cos\langle \boldsymbol{\theta}_i, \boldsymbol{\Delta} \rangle)|}{\|\sum_{i=1}^N \boldsymbol{\theta}_i\|} = \frac{\beta}{\gamma \sigma} \cdot \|\boldsymbol{\Delta}\| \left| \frac{\|\boldsymbol{\theta}_1\| \cos\langle \boldsymbol{\theta}_1, \boldsymbol{\Delta} \rangle + \dots + \|\boldsymbol{\theta}_N\| \cos\langle \boldsymbol{\theta}_N, \boldsymbol{\Delta} \rangle}{\|\boldsymbol{\theta}_1 + \dots + \boldsymbol{\theta}_N\|} \right|, \end{aligned} \quad (\text{II.5})$$

Now we make 2 assumptions:

1. The parameters $\boldsymbol{\theta}_i$ of these modes hold similar norms: $\|\boldsymbol{\theta}_1\| \approx \|\boldsymbol{\theta}_2\| \approx \dots \approx \|\boldsymbol{\theta}_N\|$.
2. The parameters $\boldsymbol{\theta}_i$ of these modes are along one nearly consistent direction, *i.e.*, the angle between any 2 different parameters $\boldsymbol{\theta}_i$ and $\boldsymbol{\theta}_j$ is nearly 0.

Then,

$$\begin{aligned} \frac{\mathcal{G}_{avg}}{\mathcal{G}_{ens}} &= \frac{|\cos\langle \boldsymbol{\theta}_1, \boldsymbol{\Delta} \rangle| + \dots + |\cos\langle \boldsymbol{\theta}_N, \boldsymbol{\Delta} \rangle|}{\|\boldsymbol{\theta}_1\| \cos\langle \boldsymbol{\theta}_1, \boldsymbol{\Delta} \rangle + \dots + \|\boldsymbol{\theta}_N\| \cos\langle \boldsymbol{\theta}_N, \boldsymbol{\Delta} \rangle} \cdot \frac{\|\boldsymbol{\theta}_1 + \dots + \boldsymbol{\theta}_N\|}{N} \\ &= \frac{|\cos\langle \boldsymbol{\theta}_1, \boldsymbol{\Delta} \rangle| + \dots + |\cos\langle \boldsymbol{\theta}_N, \boldsymbol{\Delta} \rangle|}{|\cos\langle \boldsymbol{\theta}_1, \boldsymbol{\Delta} \rangle| + \dots + \cos\langle \boldsymbol{\theta}_N, \boldsymbol{\Delta} \rangle} \geq 1. \end{aligned} \quad (\text{II.6})$$

The Proposition 1 is proved. \square

III Experiment setup details

Remark In this section, we give the thorough training details of the modes in this paper. Particularly, to obtain multiple independent modes, it is required to re-train multiple models from scratch on CIFAR10 and ImageNet *w.r.t* different random seeds. For checkable reproducibility of the results reported in this paper, all the training and evaluation code and the trained models are released² publicly.

²<https://github.com/fanghenshaometeor/ood-mode-ensemble>

network	capacity	mode-1	mode-2	mode-3	mode-4	mode-5	mode-6	mode-7	mode-8	mode-9	mode-10
RN18	11,173,962	93.21	93.33	93.61	93.26	93.68	93.57	93.60	93.85	93.79	93.91
WRN28X10	36,489,290	94.02	94.30	93.54	94.12	94.29	93.80	94.39	94.01	94.27	94.03

Table IV.1: The classification accuracy (%) of 10 isolated modes of 2 network structures, **RN18** and **WRN28X10**, on the **CIFAR10** test set as the in-distribution data.

network	capacity	mode-1	mode-2	mode-3	mode-4	mode-5
RN50	25,557,032	74.84	74.71	74.86	74.65	74.80
DN121	7,978,856	74.25	74.30	74.46	74.29	74.33
T2T-ViT-14	21,545,550	81.30	81.44	81.53	-	-

Table IV.2: The classification accuracy (%) of 5 isolated modes of 2 network structures, **RN50** and **DN121**, and 3 isolated modes of **T2T-ViT-14**, on the **ImageNet** validation set as the in-distribution data.

For the 10 independent modes of ResNet18 and Wide ResNet28x10 trained on CIFAR10, each DNN is optimized via SGD for 150 epochs with a batch size of 256 and weight decay 10^{-4} . The initial learning rate is 0.1 and reduced via a cosine scheduler to 0 during training. Each DNN is trained on one single NVIDIA GeForce RTX 3090 GPU.

For the 5 independent modes of ResNet50 and DenseNet121 trained from scratch on ImageNet, we follow the official training script³ provided by PyTorch. Each DNN is optimized via SGD for 90 epochs with weight decay 10^{-4} . The initial learning rate is 0.1 and reduced every 30 epochs by a factor of 10. The batch size for training ResNet50 and DenseNet121 is 1000 and 800, respectively. Each training is executed parallelly on 4 NVIDIA v100 GPUs.

For the 3 independent modes of T2T-ViT-14 [33] trained from scratch on ImageNet, we follow the training script provided from the official github repository⁴ and adopt the default recommendation settings. Each T2T-ViT-14 model is trained parallelly on 8 NVIDIA v100 GPUs for 310 epochs with a batch size of 64, an initial learning rate of 5×10^{-4} and weight decay 0.05.

The final models after the training finishes are evaluated for OoD detection in inference. All the training, inference and detection experiments in relation to ImageNet are executed with a resolution of $224 \times 224 \times 3$.

IV Comprehensive empirical results

In this section, the comprehensive empirical results on OoD detection covering all the detectors, network structures and data sets are provided. The recognition results on the in-distribution test data of all the modes trained on CIFAR10 and ImageNet are shown in Sec.IV.1. Sec.IV.2 and Sec.IV.3 illustrate the complete OoD detection results of each single mode and mode ensemble, respectively. The OoD detection results on the prevailing network structure, vision transformer, are presented in Sec.IV.4. The comparisons with other ensemble methods for OoD detection can be found in Sec.IV.5.

IV.1 Classification accuracy on in-distribution data

The classification accuracy of all the independent modes on their in-distribution data set CIFAR10 and ImageNet is presented in Tab.IV.1 and Tab.IV.2, respectively. It is clearly shown that these isolated modes all hold consistently good recognition performance on their corresponding in-distribution test set.

IV.2 OoD detection results of single modes

In this section, we provide the complete detection results on the OoD data sets of all single modes of different network structures trained on the CIFAR10 and ImageNet *w.r.t* different types of detectors.

Results on CIFAR10. In Tab.IV.5 and Tab.IV.6, we record the detection performance of 10 isolated modes trained on CIFAR10 of ResNet18 and Wide ResNet28X10, respectively. The **best** and **worst** detection results are marked in the 2 tables for each mode on each OoD data set *w.r.t* 5 OoD detectors: MSP, ODIN, Energy, Mahalanobis and kNN.

³<https://github.com/pytorch/examples/tree/main/imagenet>

⁴<https://github.com/yitu-opensource/T2T-ViT>

As shown in Tab.IV.5 and Tab.IV.6, those isolated and independent modes clearly hold significantly varied OoD detection results on multiple OoD data sets for different types of OoD detectors. Taking the MSP method of ResNet18 as an example, the FPR values on the SVHN data set could range from the worst 77.76% to the best 65.20% with a 12.56% difference among the 10 modes. Besides, considering the mode-4 of ResNet18, ODIN achieves lower FPR values on SVHN (55.85%) than MSP (66.45%), while for mode-9, MSP (67.52%) instead outperforms ODIN (72.09%). The results of other OoD detectors on other OoD data sets all manifest such a common phenomenon, *i.e.*, a high variance on the OoD detection performance among the isolated and independent modes, which further indicates the high uncertainty of the detection performance on OoD data for single modes.

Results on ImageNet. In Tab.IV.7 and Tab.IV.8, we record the detection performance of 5 isolated modes trained from scratch on ImageNet of ResNet50 and DenseNet121, respectively. The **best** and **worst** detection results are marked in the 2 tables for each mode on each OoD data set *w.r.t* 6 OoD detectors: MSP, ODIN, Energy, GradNorm, Mahalanobis and RankFeat.

As shown in Tab.IV.7 and Tab.IV.8, compared to the results on CIFAR10, those isolated and independent modes shows relatively more consistent detection performance. This might be due to that the training set size of ImageNet (1,281,167) is much more larger than that of CIFAR10 (50,000), which benefits the model generalization both on InD data and OoD data as the model has “seen” much more numerous images during training. Nevertheless, the detection variances among those modes cannot be simply ignored. We reiterate the 2 phenomena that reflect the high detection variances existed in the independent modes on both CIFAR10 and ImageNet, which has been summarized in the manuscript:

- For a given OoD detection method, those independent modes hold significantly-fluctuating FPR results.
- For different modes, detection results among those detection methods can also be opposite. That is, detector A might outperform detector B on some mode, while detector B shows superiority over detector A on another mode.

IV.3 OoD detection results of mode ensemble

In this section, we provide the complete detection results on the OoD data sets of ensembling multiple independent modes of different network structures on CIFAR10 and ImageNet *w.r.t* different types of detectors. The details of ensembling ways for each OoD detector have been elaborated in Sec.I.

Results on CIFAR10. For the 10 independent modes on CIFAR10, we ensemble $k \in \{1, 2, 4, 6, 8\}$ modes to verify the effectiveness of mode ensemble for OoD detection, shown in Tab.IV.9 and Tab.IV.10 for ResNet18 and Wide ResNet28X10, respectively. For $k = 1$, we report the average detection results of the total 10 modes with the mean values and standard deviations. For $k \in \{2, 4, 6, 8\}$, we randomly pick out k *different* modes from the 10 modes and perform mode ensemble, which is repeated 3 times, then the average detection results of the 3 random pickings are presented with the mean values and standard deviations.

As shown in Tab.IV.9 and Tab.IV.10, by ensembling multiple isolated modes, the variances of the detection results get reduced and the detection performance gets significantly improved. Taking the Mahalanobis method with ResNet18 as an example, its average detection FPR on SVHN of single modes is up to 24.66%, which is improved to 3.81% with a 20.85% reduction by ensembling 8 modes, while the variance simultaneously gets reduced from 12.72% to 0.52%.

Results on ImageNet. For the 5 independent modes on ImageNet, we ensemble $k \in \{1, 2, 3, 4\}$ modes to verify the effectiveness of mode ensemble for OoD detection, shown in Tab.IV.11 and Tab.IV.12 for ResNet50 and DenseNet121, respectively. For $k = 1$, we report the average detection results of the total 5 modes with the mean values and standard deviations. For $k \in \{2, 3, 4\}$, we randomly pick out k *different* modes from the 5 modes and perform mode ensemble, which is repeated 3 times, then the average detection results of the 3 random pickings are presented with the mean values and standard deviations.

As shown in Tab.IV.11 and Tab.IV.12, the mode ensemble could bring variance reduction and performance improvements for different OoD detectors. For example, considering the RankFeat method with DenseNet121, the average and the standard deviation of the detection FPR values on iNaturalist could be improved from 63.06% to 40.92% with a 22.14% reduction and from 13.98% to 5.41% with an 8.57% reduction, respectively.

In short, these detection results on both CIFAR10 and ImageNet with various OoD detectors and network structures have shown the 2 benefits brought by mode ensemble:

- For a given OoD detection method, its performance gets significantly improved via mode ensemble with both reduced variances and better detection results.

Ensemble of k modes	Method	OoD data sets											
		SVHN		LSUN		iSUN		Texture		Places365		AVERAGE	
		FPR↓	AUROC↑	FPR↓	AUROC↑	FPR↓	AUROC↑	FPR↓	AUROC↑	FPR↓	AUROC↑	FPR↓	AUROC↑
MSP													
$k = 2$	ZODE	74.47	86.91	50.68	92.90	52.44	93.08	62.57	90.06	62.22	88.89	60.48	90.37
	ours	72.64	86.88	49.05	93.12	51.88	92.98	61.15	90.01	60.08	89.09	58.96	90.42
$k = 4$	ZODE	69.85	89.49	44.71	93.67	49.76	93.28	58.24	91.23	58.77	89.50	56.27	91.43
	ours	64.69	89.58	45.34	93.54	52.96	92.49	57.36	91.05	58.21	89.53	55.71	91.24
ODIN													
$k = 2$	ZODE	75.74	83.48	23.52	96.13	34.53	95.05	54.36	89.57	48.14	89.91	47.26	90.83
	ours	72.86	83.66	24.70	95.75	36.90	94.65	50.92	89.93	47.31	89.81	46.64	90.76
$k = 4$	ZODE	75.50	88.98	16.60	97.57	21.89	97.01	51.93	91.63	45.72	91.36	42.33	93.31
	ours	63.13	89.78	15.36	97.30	23.08	96.42	44.10	91.87	40.80	91.34	37.29	93.34
Energy													
$k = 2$	ZODE	72.76	87.78	24.31	96.36	27.22	96.00	58.09	90.03	48.01	90.48	46.08	92.13
	ours	71.68	87.22	21.85	96.31	23.84	96.03	51.05	90.43	44.08	90.60	42.50	92.12
$k = 4$	ZODE	72.85	88.73	23.14	96.63	39.98	94.67	55.32	91.38	47.53	91.03	47.76	92.49
	ours	61.06	89.30	19.83	96.55	33.65	94.80	44.91	91.76	41.44	91.13	40.18	92.71
Mahalanobis													
$k = 2$	ZODE	21.73	95.53	64.32	84.29	11.94	96.49	50.82	76.88	86.90	69.68	47.14	84.57
	ours	17.55	95.59	55.33	86.17	14.10	95.36	59.33	69.93	87.60	69.93	46.78	83.40
$k = 4$	ZODE	14.17	97.36	69.28	82.88	6.26	98.73	29.26	93.17	88.44	70.70	41.46	88.57
	ours	4.65	98.90	76.00	74.98	10.57	97.66	28.17	91.00	86.71	73.34	41.22	87.18

Table IV.3: Comparisons between ZODE and ours on ensembling k modes (ResNet18 trained on CIFAR10) on each OoD data set *w.r.t* different OoD detectors.

- Mode ensemble also benefits the evaluation among different OoD detectors as it gets rid of the uncertainties of single modes.

IV.4 OoD detection results on vision transformer

In this section, the OoD detection performance on the popular network structure of the vision transformer is presented in Tab.IV.13 involving both single modes and mode ensemble ($k = 2$), where each single mode is trained on ImageNet from scratch with much longer training time (310 epochs).

As shown in Tab.IV.13, for the powerful generalization ability of T2T-ViT-14, there exist even smaller detection variances of multiple isolated modes, especially for those logits-based detectors (MSP, ODIN and Energy). Even though, those features-based detectors, especially RankFeat, still hold very high variances among independent modes. On the other hand, mode ensemble always brings variance reduction and substantial performance improvements for different OoD detectors, shown in Tab.IV.13.

IV.5 Comparison with other ensemble detection methods

In the ablation studies in the manuscript, we have compared the detection performance between ensembling independent modes and dependent modes. In this section, the proposed mode ensemble is further compared with another type of ensemble for OoD detection: ZODE [24]. Different from ensembling the output logits or features in DNNs of our method, ZODE proposes to perform ensemble on the p-values from multiple models, where the p-values are calculated from the detection scores. Accordingly, the key difference between our mode ensemble and ZODE is,

- In ours, the outputs (logits or features) from multiple modes are firstly get ensembled, and then the detection score is computed based on the ensembled outputs to decide the OoD prediction.
- In ZODE, the detection score of each individual model is firstly determined to calculate the p-value, and then those p-values from multiple models get ensembled to decide the OoD prediction.

Tab.IV.3 and Tab.IV.4 present the comparison results in OoD detection between ZODE and ours on CIFAR10 and ImageNet, respectively. For a fair comparison, in each experiment, both ZODE and ours adopt the same OoD detectors on the same models that are trained as elaborated in Sec.III.

As shown in Tab.IV.3 and Tab.IV.4, under different OoD detectors and different numbers of ensembled models, our mode ensemble method generally outperforms ZODE in terms of the average FPR values on multiple OoD data sets. Such results indicate that ensembling the output features or logits from multiple DNNs might be a better choice than

Ensemble of k modes	Method	OoD data sets									
		iNaturalist		SUN		Places		Textures		AVERAGE	
		FPR↓	AUROC↑	FPR↓	AUROC↑	FPR↓	AUROC↑	FPR↓	AUROC↑	FPR↓	AUROC↑
MSP											
$k = 2$	ZODE	56.40	88.68	69.63	82.28	71.70	81.43	63.58	82.75	65.33	83.79
	ours	55.85	88.01	68.44	81.99	70.78	81.21	63.42	81.60	64.62	83.20
$k = 4$	ZODE	56.02	90.00	70.80	82.81	73.45	81.89	64.13	83.96	66.10	84.67
	ours	52.86	89.06	68.65	82.35	70.81	81.54	63.99	82.06	64.08	83.75
ODIN											
$k = 2$	ZODE	57.13	90.15	60.61	86.79	65.24	84.69	51.70	88.22	58.67	87.46
	ours	52.77	90.58	58.28	86.92	62.15	84.94	49.17	88.37	55.59	87.70
$k = 4$	ZODE	56.38	91.65	60.86	87.82	65.70	85.93	51.45	89.06	58.60	88.62
	ours	48.04	92.03	55.26	87.88	60.09	86.07	46.93	89.05	52.58	88.76
Energy											
$k = 2$	ZODE	57.55	89.78	55.38	87.72	61.16	85.67	47.62	88.65	55.43	87.96
	ours	53.22	90.39	52.64	87.88	58.32	85.94	44.66	88.86	52.21	88.27
$k = 4$	ZODE	56.27	91.12	57.95	88.08	64.50	85.79	48.42	89.61	56.79	88.65
	ours	48.14	91.84	52.26	88.25	58.87	86.08	43.07	89.85	50.59	89.01
Mahalanobis											
$k = 2$	ZODE	92.00	61.54	88.50	68.85	87.45	71.05	44.40	74.42	78.09	68.97
	ours	87.65	65.43	81.10	74.54	81.20	75.02	39.43	78.06	72.35	73.26
$k = 4$	ZODE	94.10	62.72	90.77	69.80	89.58	72.23	46.17	74.44	80.16	69.80
	ours	79.60	71.33	77.54	79.12	80.09	76.72	33.16	85.21	67.60	78.10

Table IV.4: Comparisons between ZODE and ours on ensembling k modes (DenseNet121 trained on ImageNet) on each OoD data set *w.r.t* different OoD detectors.

ensembling the scores from multiple DNNs in OoD detection, since features or logits could contain more useful and diversified information than the decision scores.

Table IV.5: The detection performance of each mode of **ResNet18** trained on **CIFAR10** w.r.t 5 OoD detectors: MSP, ODIN, Energy, Mahalanobis and kNN. The **best** and **worst** results of each mode on each OoD data set are highlighted.

Modes	OoD data sets									
	SVHN		LSUN		iSUN		Texture		Places365	
	FPR↓	AUROC↑	FPR↓	AUROC↑	FPR↓	AUROC↑	FPR↓	AUROC↑	FPR↓	AUROC↑
MSP										
mode-1	74.87	83.87	55.00	91.70	52.67	92.09	67.36	87.26	64.57	87.60
mode-2	71.58	86.86	53.19	92.07	65.85	88.92	65.07	88.25	65.23	87.76
mode-3	74.87	83.69	56.30	90.94	63.74	90.17	64.79	88.53	65.61	87.46
mode-4	66.45	89.15	50.01	92.52	61.85	90.21	65.66	88.63	64.97	87.84
mode-5	73.32	84.69	48.30	93.19	60.86	89.45	63.10	88.60	63.14	87.78
mode-6	65.20	89.09	51.25	92.44	59.88	90.84	61.60	89.92	63.56	87.89
mode-7	77.26	86.00	50.81	92.50	65.21	88.74	63.21	88.31	63.53	87.55
mode-8	77.76	83.30	51.12	92.57	49.45	93.02	63.63	88.64	63.32	87.88
mode-9	67.52	88.83	51.82	92.92	60.04	90.82	64.06	88.79	64.69	87.68
mode-10	68.01	89.65	43.08	94.07	58.68	90.86	63.39	88.88	62.83	88.30
ODIN										
mode-1	72.98	81.82	26.70	95.39	23.53	96.00	62.57	85.74	48.04	89.34
mode-2	71.33	84.87	25.16	95.58	44.21	92.46	60.07	86.45	48.93	89.11
mode-3	76.52	79.16	29.63	94.30	34.76	94.39	54.88	87.94	50.48	88.42
mode-4	55.85	88.81	22.09	95.73	37.85	93.32	55.46	87.91	47.74	88.95
mode-5	67.92	85.33	18.83	96.85	41.10	91.95	54.91	87.93	49.03	88.89
mode-6	59.50	88.21	21.29	96.18	35.20	93.81	48.12	90.27	45.59	89.45
mode-7	72.02	83.45	21.28	96.22	39.91	93.54	56.08	86.98	48.89	88.52
mode-8	82.60	79.29	25.15	95.77	23.19	96.02	56.76	87.82	48.49	89.18
mode-9	72.09	84.64	20.23	96.36	37.41	93.80	56.21	87.02	48.04	88.84
mode-10	67.90	88.65	14.53	97.38	32.59	94.64	54.77	88.15	46.09	90.00
Energy										
mode-1	74.86	81.63	28.78	95.09	26.66	95.52	63.67	85.87	47.89	89.49
mode-2	75.22	84.76	27.84	95.33	48.77	91.66	62.07	86.67	49.45	89.32
mode-3	78.63	79.66	30.99	94.19	39.16	93.66	55.05	88.27	50.34	88.65
mode-4	59.05	89.01	24.01	95.62	43.03	92.66	57.71	88.06	48.81	89.15
mode-5	70.56	85.11	21.06	96.57	44.22	91.24	55.92	88.10	48.84	89.12
mode-6	62.67	88.40	22.73	96.02	39.92	92.96	49.54	90.37	45.73	89.64
mode-7	72.61	84.10	22.03	96.12	43.70	92.61	56.49	87.42	48.55	88.84
mode-8	84.44	79.21	27.99	95.51	27.46	95.54	57.91	88.01	49.23	89.32
mode-9	75.91	84.69	22.33	96.23	42.75	93.06	57.91	87.44	48.62	89.09
mode-10	71.11	88.51	15.04	97.32	35.31	94.09	55.27	88.49	46.33	90.10
Mahalanobis										
mode-1	38.26	89.52	68.10	78.51	15.05	93.92	69.15	57.90	92.69	59.35
mode-2	45.30	89.92	75.27	75.85	64.41	75.46	38.79	87.48	92.39	65.74
mode-3	11.22	97.21	75.15	60.15	10.32	97.21	27.94	89.78	87.71	62.28
mode-4	25.49	92.30	75.58	79.01	8.89	97.87	51.21	74.12	86.43	69.90
mode-5	15.48	96.31	84.38	54.03	85.47	44.85	31.72	87.74	89.92	62.33
mode-6	40.42	88.16	79.89	69.72	4.53	98.62	59.96	67.98	89.56	65.15
mode-7	25.64	93.61	72.10	78.23	30.16	88.87	58.30	70.00	82.43	72.59
mode-8	10.40	97.54	67.36	77.06	8.32	97.82	36.19	86.61	91.67	61.73
mode-9	20.13	94.30	73.10	79.27	13.13	95.93	42.39	80.21	84.74	69.65
mode-10	14.29	96.68	82.36	63.37	13.78	97.18	22.18	94.04	87.33	67.13
kNN										
mode-1	44.24	93.56	39.55	94.08	33.92	94.41	42.96	92.42	53.70	88.31
mode-2	48.67	92.34	40.68	93.45	42.04	92.91	45.59	92.15	52.67	89.07
mode-3	48.96	92.23	38.15	93.80	38.66	93.58	41.37	92.74	52.82	88.74
mode-4	50.08	92.34	41.41	93.33	37.71	93.73	45.55	92.35	53.86	89.07
mode-5	62.06	89.79	38.08	94.16	39.75	93.25	41.26	92.95	52.10	89.08
mode-6	41.03	93.48	50.43	92.37	37.08	93.84	41.86	93.02	53.13	88.93

Continued on next page

Table IV.5 – continued from previous page

Modes	SVHN		LSUN		OoD data sets iSUN		Texture		Places365	
	FPR↓	AUROC↑	FPR↓	AUROC↑	FPR↓	AUROC↑	FPR↓	AUROC↑	FPR↓	AUROC↑
mode-7	71.17	89.38	42.01	93.49	45.18	92.24	42.73	92.80	53.37	88.71
mode-8	66.00	90.28	41.60	93.92	31.11	95.12	44.91	92.67	53.02	88.94
mode-9	38.29	94.33	36.58	94.49	40.45	93.54	39.26	93.37	53.64	88.76
mode-10	36.87	94.43	32.10	94.96	38.49	93.46	40.44	92.86	51.84	88.90

Table IV.6: The detection performance of each mode of **Wide ResNet28X10** trained on **CIFAR10** w.r.t 5 OoD detectors: MSP, ODIN, Energy, Mahalanobis and kNN. The **best** and **worst** results of each mode are highlighted.

Modes	SVHN		LSUN		OoD data sets iSUN		Texture		Places365	
	FPR↓	AUROC↑	FPR↓	AUROC↑	FPR↓	AUROC↑	FPR↓	AUROC↑	FPR↓	AUROC↑
MSP										
mode-1	54.52	93.54	32.95	95.66	46.82	93.59	60.90	89.12	62.48	88.44
mode-2	30.10	95.62	27.41	96.29	52.13	92.71	64.04	88.08	57.17	89.84
mode-3	45.38	94.01	23.21	96.57	47.41	93.58	53.65	90.95	62.54	88.12
mode-4	60.18	91.23	32.71	95.80	52.25	92.83	62.27	89.82	62.00	88.22
mode-5	43.60	94.00	26.34	96.25	52.25	92.77	60.55	89.30	59.62	89.06
mode-6	37.53	94.38	17.96	97.26	40.64	94.23	48.32	91.76	59.19	88.83
mode-7	53.86	92.12	27.23	96.13	40.19	94.46	60.30	88.03	57.34	89.55
mode-8	44.99	94.24	21.92	96.85	66.53	89.79	62.45	88.59	57.71	89.76
mode-9	46.18	93.92	24.57	96.37	42.10	93.92	53.65	91.36	60.16	88.85
mode-10	31.58	95.65	28.90	95.97	49.74	93.22	57.38	90.50	59.94	88.64
ODIN										
mode-1	24.29	96.09	6.86	98.71	21.27	96.40	48.85	89.21	47.49	89.76
mode-2	16.52	96.93	6.00	98.87	25.88	96.07	54.10	88.20	38.79	92.22
mode-3	20.24	96.46	5.37	98.93	19.71	96.66	37.52	92.30	50.40	89.25
mode-4	44.97	92.36	6.26	98.76	30.67	94.94	52.73	88.95	49.23	88.77
mode-5	23.83	96.05	5.26	98.94	24.27	96.01	50.32	89.01	46.48	90.08
mode-6	22.12	96.40	3.50	99.28	21.56	96.45	37.09	92.40	46.72	90.26
mode-7	45.82	92.34	5.45	98.85	19.61	96.44	52.73	86.02	39.11	91.36
mode-8	20.86	96.54	3.63	99.24	36.62	94.38	52.30	88.72	38.53	92.16
mode-9	25.96	95.85	5.36	98.87	16.96	96.81	39.18	92.32	43.67	90.67
mode-10	13.69	97.61	7.46	98.68	27.27	95.63	45.16	90.95	46.06	89.97
Energy										
mode-1	24.22	96.09	7.44	98.60	25.33	95.77	49.88	89.03	47.43	89.83
mode-2	15.78	97.05	6.20	98.83	32.44	95.15	55.51	88.01	38.80	92.22
mode-3	18.99	96.66	6.08	98.85	23.92	96.03	39.49	91.97	50.79	89.25
mode-4	42.75	92.76	6.56	98.69	37.20	94.04	53.76	88.87	49.48	88.92
mode-5	23.37	96.07	5.92	98.84	28.71	95.37	51.24	88.95	46.71	90.17
mode-6	21.94	96.38	3.85	99.21	25.64	95.86	38.51	92.12	47.43	90.18
mode-7	48.05	92.23	5.85	98.77	24.86	96.58	55.21	86.00	39.19	91.44
mode-8	20.87	96.57	3.96	99.19	43.41	93.37	54.26	88.41	38.55	92.22
mode-9	25.18	96.02	6.32	98.78	20.65	96.31	40.51	92.17	44.65	90.65
mode-10	12.43	97.74	7.48	98.65	34.35	94.67	47.18	90.58	45.87	90.10
Mahalanobis										
mode-1	3.91	99.09	63.06	82.65	5.47	98.65	16.77	95.07	81.80	72.57
mode-2	6.94	98.46	79.02	74.97	5.93	98.65	24.36	93.41	86.63	68.60
mode-3	10.93	97.44	77.92	76.55	9.28	97.67	28.99	91.06	86.27	66.88
mode-4	2.94	99.20	67.43	78.59	6.23	98.39	17.73	94.48	82.10	72.09
mode-5	5.69	98.68	67.35	81.57	5.46	98.63	22.73	93.21	84.45	70.65
mode-6	64.41	86.19	90.87	65.72	10.91	96.79	46.19	83.97	89.61	65.51
mode-7	6.81	98.55	78.26	76.43	6.31	98.40	24.59	92.87	85.76	69.93

Continued on next page

Table IV.6 – continued from previous page

Modes	OoD data sets										
	SVHN		LSUN		iSUN		Texture		Places365		
	FPR↓	AUROC↑	FPR↓	AUROC↑	FPR↓	AUROC↑	FPR↓	AUROC↑	FPR↓	AUROC↑	
mode-8	4.36	98.93	70.49	77.11	6.83	98.37	18.03	94.39	83.65	70.72	
mode-9	7.86	98.09	73.04	76.48	6.32	98.36	22.89	93.34	85.01	68.50	
mode-10	6.80	98.37	71.34	78.83	4.95	98.71	23.09	92.81	85.54	69.15	
					kNN						
mode-1	30.51	95.48	21.47	96.45	21.94	96.34	36.21	94.21	47.06	90.22	
mode-2	17.35	97.22	21.79	96.52	28.21	95.47	42.64	92.79	43.30	91.28	
mode-3	22.78	96.58	18.43	96.90	26.95	95.74	30.60	95.16	50.97	89.44	
mode-4	25.12	96.25	23.10	96.36	32.10	94.92	37.71	94.07	47.83	89.97	
mode-5	25.78	96.27	21.75	96.58	32.06	95.01	35.76	94.19	45.94	90.73	
mode-6	22.78	96.36	15.21	97.50	21.50	96.39	28.51	95.29	48.39	89.59	
mode-7	30.43	95.51	19.72	96.87	18.17	96.91	40.94	93.67	42.11	91.48	
mode-8	19.10	96.94	19.41	96.87	42.07	92.89	45.20	92.38	42.51	91.43	
mode-9	22.45	96.58	19.18	97.00	26.43	95.73	31.84	94.84	50.16	89.90	
mode-10	17.18	97.37	22.28	96.35	19.31	96.78	31.31	94.93	46.00	90.39	

Modes	OoD data sets							
	iNaturalist		SUN		Places		Texture	
	FPR↓	AUROC↑	FPR↓	AUROC↑	FPR↓	AUROC↑	FPR↓	AUROC↑
MSP								
mode-1	57.33	87.29	70.84	80.65	72.49	80.44	67.20	81.10
mode-2	55.43	87.95	70.50	81.35	72.82	80.43	69.54	79.88
mode-3	55.84	87.89	70.06	81.11	72.63	80.31	65.89	81.04
mode-4	55.95	87.49	70.81	80.70	72.96	80.15	68.33	79.84
mode-5	<u>59.73</u>	<u>86.87</u>	<u>71.55</u>	80.80	<u>72.34</u>	80.29	69.08	80.38
ODIN								
mode-1	53.69	90.15	60.23	86.32	63.79	84.89	55.34	86.40
mode-2	52.80	90.31	59.09	87.05	62.72	85.07	57.62	85.39
mode-3	53.01	90.28	58.66	86.80	63.78	84.73	53.39	86.50
mode-4	54.39	89.90	60.11	85.99	64.90	84.33	57.27	85.00
mode-5	<u>56.56</u>	<u>89.55</u>	<u>60.28</u>	86.17	63.45	84.68	56.12	85.76
Energy								
mode-1	56.13	89.61	58.21	86.63	62.27	84.99	53.78	86.61
mode-2	56.06	89.64	56.88	87.37	61.85	85.21	55.53	85.63
mode-3	56.35	89.54	56.44	87.08	62.50	84.80	51.44	86.76
mode-4	57.70	89.22	58.62	86.23	63.58	84.36	55.67	85.19
mode-5	<u>59.45</u>	<u>88.90</u>	<u>58.75</u>	86.42	62.62	84.78	54.49	85.98
GradNorm								
mode-1	57.90	83.27	63.94	79.64	71.55	75.51	59.72	79.85
mode-2	53.97	85.28	63.82	80.08	72.09	75.86	62.39	78.32
mode-3	52.03	85.71	61.13	80.78	70.67	76.26	55.05	81.10
mode-4	57.42	83.62	64.47	78.40	73.30	74.34	61.01	78.18
mode-5	<u>63.03</u>	<u>81.45</u>	<u>67.78</u>	78.02	74.47	74.43	61.95	78.79
Mahalanobis								
mode-1	96.66	54.33	97.38	49.83	96.95	50.44	36.79	85.52
mode-2	95.04	59.89	96.35	53.62	96.05	51.92	33.87	88.19
mode-3	97.06	48.77	96.63	50.74	96.23	52.32	45.90	74.52
mode-4	97.35	48.14	96.85	50.56	96.10	53.33	44.80	75.80
mode-5	<u>97.58</u>	46.06	96.99	48.11	96.12	51.20	53.74	67.49
RankFeat								
mode-1	83.89	71.16	79.96	76.63	83.18	72.18	55.05	85.81
mode-2	78.78	72.18	80.51	76.56	85.82	71.56	65.78	78.05
mode-3	95.46	46.77	80.17	76.74	84.16	71.89	72.94	73.83
mode-4	94.02	55.37	94.02	59.55	94.49	56.68	71.67	76.61
mode-5	78.26	70.35	76.58	77.42	81.29	72.41	53.71	85.48

Table IV.7: The detection performance of each of the 5 modes of **ResNet50** trained from scratch on **ImageNet w.r.t 6** OoD detectors: MSP, ODIN, Energy, GradNorm, Mahalanobis and RankFeat. The **best** and **worst** results of each mode on each OoD data set are highlighted.

Modes	OoD data sets							
	iNaturalist		SUN		Places		Texture	
	FPR↓	AUROC↑	FPR↓	AUROC↑	FPR↓	AUROC↑	FPR↓	AUROC↑
MSP								
mode-1	58.44	87.18	<u>71.11</u>	80.78	<u>74.11</u>	<u>79.69</u>	67.07	80.72
mode-2	<u>55.68</u>	<u>87.28</u>	<u>68.78</u>	<u>81.49</u>	<u>70.85</u>	<u>80.63</u>	66.21	<u>80.27</u>
mode-3	58.29	87.10	70.60	81.02	73.01	80.07	66.06	80.70
mode-4	58.52	87.20	70.73	80.81	72.79	79.77	<u>67.85</u>	80.46
mode-5	<u>60.97</u>	<u>86.19</u>	70.82	<u>80.69</u>	72.76	79.89	<u>64.41</u>	<u>80.93</u>
ODIN								
mode-1	54.88	89.39	<u>60.26</u>	<u>85.76</u>	<u>65.84</u>	<u>83.33</u>	54.36	86.61
mode-2	<u>50.56</u>	90.21	<u>55.79</u>	<u>87.00</u>	<u>60.81</u>	<u>85.08</u>	53.35	<u>86.62</u>
mode-3	51.61	90.12	57.90	86.08	63.82	<u>85.08</u>	53.35	<u>86.62</u>
mode-4	51.47	<u>90.26</u>	59.03	86.28	63.56	84.01	<u>55.12</u>	86.20
mode-5	<u>58.13</u>	<u>88.39</u>	59.17	85.84	63.17	84.07	<u>51.83</u>	<u>86.19</u>
Energy								
mode-1	56.24	88.63	<u>57.85</u>	<u>85.99</u>	<u>64.35</u>	<u>83.29</u>	51.93	86.98
mode-2	<u>52.86</u>	89.67	<u>53.31</u>	<u>87.32</u>	<u>59.77</u>	<u>85.16</u>	50.76	<u>87.05</u>
mode-3	53.19	89.61	55.89	86.35	62.05	84.13	50.64	86.86
mode-4	53.31	<u>89.77</u>	56.85	86.58	62.75	84.08	<u>53.56</u>	86.53
mode-5	<u>60.92</u>	<u>87.56</u>	56.76	86.07	61.93	84.11	<u>49.93</u>	<u>86.46</u>
GradNorm								
mode-1	73.79	77.93	72.64	75.03	<u>81.21</u>	70.23	66.15	77.82
mode-2	69.99	79.89	<u>68.30</u>	76.72	<u>75.71</u>	72.63	<u>63.30</u>	<u>78.74</u>
mode-3	69.93	79.67	69.12	<u>77.56</u>	77.22	<u>73.34</u>	64.06	78.48
mode-4	<u>66.85</u>	<u>81.07</u>	72.51	75.61	80.08	71.44	65.87	77.27
mode-5	<u>77.07</u>	<u>73.47</u>	<u>73.66</u>	<u>73.88</u>	80.59	<u>69.90</u>	<u>66.83</u>	<u>76.39</u>
Mahalanobis								
mode-1	89.20	63.79	84.50	<u>70.98</u>	83.84	71.65	<u>43.56</u>	<u>75.46</u>
mode-2	<u>93.31</u>	60.90	85.98	68.14	83.87	71.11	<u>65.21</u>	<u>58.26</u>
mode-3	<u>88.43</u>	<u>69.11</u>	86.21	70.74	85.17	72.50	51.40	70.16
mode-4	91.84	<u>58.88</u>	<u>86.82</u>	<u>66.23</u>	<u>85.54</u>	<u>69.64</u>	49.86	68.64
mode-5	92.43	59.27	<u>82.07</u>	70.24	<u>81.02</u>	<u>72.95</u>	57.20	63.21
RankFeat								
mode-1	66.01	85.91	<u>75.53</u>	<u>80.27</u>	<u>79.95</u>	<u>75.64</u>	43.60	<u>90.35</u>
mode-2	58.49	83.77	<u>34.70</u>	<u>92.02</u>	<u>50.70</u>	<u>86.12</u>	32.73	92.45
mode-3	59.53	85.17	50.07	88.37	63.27	82.05	40.64	91.54
mode-4	<u>84.70</u>	<u>78.61</u>	69.57	83.82	76.45	78.21	<u>49.89</u>	90.81
mode-5	<u>46.58</u>	<u>87.27</u>	44.46	88.42	58.95	81.54	<u>22.48</u>	<u>94.15</u>

Table IV.8: The detection performance of each of the 5 modes of **DenseNet121** trained from scratch on **ImageNet** w.r.t 6 OoD detectors: MSP, ODIN, Energy, GradNorm, Mahalanobis and RankFeat. The **best** and **worst** results of each mode on each OoD data set are highlighted.

Ensemble of k modes	SVHN		LSUN		OoD data sets iSUN		Texture		Places365	
	FPR↓	AUROC↑	FPR↓	AUROC↑	FPR↓	AUROC↑	FPR↓	AUROC↑	FPR↓	AUROC↑
MSP										
$k=1$	71.68±4.61	86.51±2.53	51.09±3.66	92.49±0.84	59.82±5.23	90.51±1.34	64.19±1.60	88.58±0.66	64.15±0.98	87.77±0.23
$k=2$	68.23±5.74	88.46±1.84	43.56±6.07	93.75±0.71	51.71±4.49	92.68±0.89	58.54±2.26	90.35±0.35	59.35±1.15	89.10±0.14
$k=4$	66.34±5.25	88.95±2.60	44.98±3.70	93.66±0.63	55.71±2.39	91.88±0.54	57.69±0.47	90.79±0.33	58.87±0.57	89.49±0.14
$k=6$	67.03±0.91	89.34±0.68	44.99±1.40	93.82±0.21	55.04±2.61	92.31±0.76	57.49±0.35	91.03±0.09	58.75±0.37	89.73±0.05
$k=8$	66.70±1.67	89.22±0.70	44.56±1.65	93.83±0.24	54.02±0.85	92.40±0.14	56.87±0.78	91.16±0.14	57.88±0.47	89.81±0.05
ODIN										
$k=1$	69.87±7.74	84.42±3.56	22.49±4.32	95.98±0.84	34.98±6.97	93.99±1.33	55.98±3.75	87.62±1.22	48.13±1.43	89.07±0.46
$k=2$	69.90±6.36	86.50±2.66	21.59±4.37	96.35±0.78	33.04±10.60	95.05±1.42	51.58±2.43	90.05±0.43	46.14±1.55	90.34±0.50
$k=4$	64.13±3.16	89.11±1.20	18.64±2.99	96.85±0.42	25.56±2.15	96.16±0.23	46.09±1.72	91.51±0.34	42.53±1.53	91.06±0.24
$k=6$	59.88±0.40	90.15±0.15	17.50±0.85	96.99±0.12	28.21±2.05	95.86±0.29	44.82±0.65	91.73±0.12	40.85±0.11	91.44±0.03
$k=8$	61.74±2.23	89.71±0.39	17.16±0.66	97.09±0.12	27.00±2.58	96.05±0.32	44.61±0.34	91.86±0.05	40.58±0.16	91.57±0.04
Energy										
$k=1$	72.51±7.36	84.51±3.53	24.28±4.70	95.80±0.86	39.10±7.26	93.30±1.44	57.15±3.89	87.87±1.19	48.38±1.40	89.27±0.41
$k=2$	64.19±6.50	88.93±1.67	18.41±3.26	96.83±0.47	31.12±6.61	94.71±1.30	48.51±2.63	90.79±0.41	42.97±0.96	90.76±0.19
$k=4$	67.45±5.59	88.20±1.32	18.83±1.87	96.83±0.33	25.86±6.93	95.97±1.04	47.01±2.15	91.44±0.43	40.96±0.57	91.41±0.25
$k=6$	63.39±1.43	89.58±0.46	17.65±1.11	97.01±0.16	29.10±0.82	95.66±0.17	45.19±0.65	91.85±0.08	40.39±0.41	91.51±0.08
$k=8$	64.21±0.90	89.67±0.42	16.55±0.08	97.19±0.05	26.17±0.75	96.09±0.07	45.24±0.60	91.84±0.11	39.73±0.19	91.72±0.08
Mahalanobis										
$k=1$	24.66±12.72	93.56±3.45	75.33±5.61	71.52±9.22	25.41±27.43	88.77±16.96	43.78±15.34	79.59±11.63	88.49±3.39	65.59±4.24
$k=2$	11.17±5.53	97.20±1.40	73.92±16.15	73.54±11.02	45.01±36.43	73.58±29.89	44.41±12.95	79.48±8.28	87.60±2.22	69.09±4.01
$k=4$	4.68±1.28	98.88±0.26	75.31±6.14	75.88±2.82	20.38±9.28	93.71±3.42	27.71±2.11	91.25±0.82	85.58±1.83	73.72±2.28
$k=6$	5.24±2.23	98.71±0.49	70.82±0.70	78.01±1.98	28.25±21.42	86.76±11.95	31.24±8.38	88.04±5.04	83.62±1.58	74.41±1.41
$k=8$	3.81±0.52	99.08±0.17	77.27±1.89	76.59±2.20	11.62±5.34	95.91±3.04	25.44±8.76	91.85±3.95	82.11±0.93	77.09±0.06
kNN										
$k=1$	50.74±11.88	92.22±1.84	40.06±4.70	93.81±0.71	38.44±3.95	93.61±0.78	42.59±2.18	92.73±0.36	53.02±0.67	88.85±0.24
$k=2$	47.14±5.67	93.19±1.26	45.19±6.06	93.17±1.02	29.78±5.46	95.43±0.75	38.42±2.04	93.79±0.29	52.82±1.31	89.36±0.14
$k=4$	48.63±6.45	92.96±0.60	52.19±1.92	91.90±0.25	31.54±2.97	95.31±0.44	35.53±1.14	94.32±0.14	53.82±1.30	89.36±0.06
$k=6$	47.35±1.55	93.41±0.34	54.81±2.41	91.58±0.57	27.49±2.09	95.89±0.21	33.82±0.47	94.64±0.12	54.70±0.29	89.40±0.12
$k=8$	47.34±0.74	93.32±0.17	57.44±0.91	91.05±0.31	28.98±0.98	95.82±0.09	35.22±0.17	94.52±0.05	56.34±0.26	89.24±0.07

Table IV.9: The detection performance of ensembling k modes (**ResNet18** trained on **CIFAR10**) on each OoD data set *w.r.t* different types of OoD detectors. The results with the **lowest variances** are highlighted with bold fonts.

Ensemble of k modes	SVHN		LSUN		OoD data sets iSUN		Texture		Places365	
	FPR↓	AUROC↑	FPR↓	AUROC↑	FPR↓	AUROC↑	FPR↓	AUROC↑	FPR↓	AUROC↑
MSP										
$k=1$	44.79±9.78	93.87±1.37	26.32±4.66	96.32±0.48	49.01±7.75	93.11±1.32	58.35±5.00	89.75±1.35	59.82±2.04	88.93±0.62
$k=2$	33.72±4.01	95.36±0.42	20.88±1.48	96.92±0.13	45.66±5.05	93.92±0.74	54.54±2.22	90.77±0.74	55.88±1.58	89.99±0.40
$k=4$	35.16±1.04	95.17±0.30	18.68±1.53	97.11±0.08	36.86±2.28	95.13±0.16	52.10±1.14	91.43±0.41	54.04±1.46	90.50±0.21
$k=6$	36.91±2.24	95.23±0.24	20.10±1.15	97.04±0.16	40.51±5.81	94.88±0.62	53.21±2.89	91.65±0.56	55.11±0.42	90.50±0.03
$k=8$	34.02±2.53	95.51±0.21	19.96±1.12	97.03±0.13	39.96±2.29	94.97±0.21	54.11±1.44	91.46±0.24	54.16±0.89	90.73±0.13
ODIN										
$k=1$	25.83±10.93	95.66±1.82	5.52±1.25	98.91±0.20	24.38±5.94	95.98±0.78	47.00±6.76	89.81±2.12	44.65±4.41	90.45±1.16
$k=2$	20.99±8.56	96.64±1.12	3.94±0.64	99.12±0.15	15.92±1.78	97.26±0.30	39.39±4.93	92.31±1.24	41.12±3.02	91.57±0.69
$k=4$	17.33±3.30	97.06±0.36	3.61±0.39	99.13±0.05	16.66±3.58	97.15±0.42	39.32±3.70	92.45±0.82	39.52±2.13	91.83±0.44
$k=6$	16.01±2.08	97.22±0.24	3.29±0.11	99.18±0.03	14.49±1.34	97.41±0.11	40.60±4.31	91.92±1.03	37.15±1.25	92.38±0.43
$k=8$	14.29±0.38	97.48±0.09	3.02±0.04	99.24±0.01	12.79±0.55	97.62±0.06	38.48±1.59	92.52±0.33	36.91±0.23	92.50±0.04
Energy										
$k=1$	25.36±11.32	95.76±1.80	5.97±1.23	98.84±0.21	29.65±7.06	95.32±1.03	48.56±6.76	89.61±2.05	44.89±4.51	90.50±1.14
$k=2$	21.86±5.03	96.39±0.67	4.52±0.82	99.04±0.13	20.28±7.02	96.59±0.85	41.99±3.83	91.55±0.82	41.42±3.51	91.27±0.79
$k=4$	11.21±1.10	97.88±0.06	3.24±0.31	99.28±0.06	16.97±1.20	97.14±0.12	39.32±2.29	92.40±0.47	37.06±2.04	92.55±0.34
$k=6$	15.28±2.01	97.28±0.28	2.96±0.39	99.29±0.07	15.07±0.54	97.30±0.08	39.31±0.72	92.24±0.25	36.86±0.85	92.39±0.15
$k=8$	13.78±1.56	97.51±0.23	2.76±0.06	99.31±0.04	13.25±0.12	97.53±0.03	38.33±0.90	92.42±0.12	36.09±0.77	92.61±0.23
Mahalanobis										
$k=1$	12.07±18.53	97.30±3.94	73.88±7.96	76.89±4.60	6.77±1.87	98.26±0.60	24.54±8.47	92.46±3.18	85.08±2.29	69.46±2.21
$k=2$	11.26±9.37	97.69±1.56	76.36±7.70	76.37±4.10	6.97±1.54	98.18±0.47	22.90±5.43	93.48±1.46	85.61±1.99	70.02±2.12
$k=4$	5.24±1.46	98.80±0.32	75.79±1.29	76.04±1.23	5.39±0.99	98.66±0.27	18.68±0.70	94.93±0.04	80.39±1.18	75.05±0.85
$k=6$	7.09±1.64	98.42±0.32	80.74±4.29	69.44±3.00	6.40±1.63	98.35±0.46	20.44±2.89	94.03±1.18	79.64±1.26	75.43±0.77
$k=8$	5.09±1.18	98.85±0.26	82.97±1.25	68.46±1.04	5.56±0.55	98.67±0.18	16.68±0.93	95.69±0.49	78.05±0.49	77.98±0.82
kNN										
$k=1$	23.35±4.76	96.46±0.63	20.23±2.34	96.74±0.36	26.87±7.25	95.62±1.18	36.07±5.58	94.15±0.98	46.43±3.07	90.44±0.76
$k=2$	17.39±1.30	97.36±0.17	16.36±0.99	97.35±0.20	21.23±6.68	96.67±0.90	29.37±4.27	95.48±0.65	43.91±1.73	91.20±0.37
$k=4$	16.61±1.50	97.56±0.19	14.67±0.07	97.74±0.02	14.48±0.72	97.60±0.06	26.00±1.64	96.05±0.19	43.44±2.23	91.53±0.38
$k=6$	13.93±0.39	97.94±0.04	14.34±0.47	97.87±0.06	13.00±1.55	97.90±0.17	23.70±0.62	96.50±0.06	43.60±1.30	91.67±0.17
$k=8$	13.57±0.34	98.04±0.07	13.74±0.19	97.97±0.04	12.71±0.49	97.96±0.09	23.48±0.09	96.58±0.02	43.87±1.13	91.75±0.16

Table IV.10: The detection performance of ensembling k modes (**Wide ResNet28X10** trained on **CIFAR10**) on each OoD data set *w.r.t* different types of OoD detectors. The results with the **lowest variances** are highlighted with bold fonts.

Ensemble of k modes	OoD data sets							
	iNaturalist		SUN		Places		Textures	
	FPR↓	AUROC↑	FPR↓	AUROC↑	FPR↓	AUROC↑	FPR↓	AUROC↑
	MSP							
$k = 1$	56.86±1.76	87.50±0.45	70.75±0.55	80.92±0.30	72.65±0.25	80.32±0.12	68.01±1.48	80.45±0.61
$k = 2$	53.08±1.10	88.64±0.29	69.41±0.39	81.71±0.12	70.79±0.22	81.18±0.11	65.46±0.63	81.44±0.26
$k = 3$	52.22±0.68	88.98±0.21	69.09±0.33	82.00±0.09	70.74±0.18	81.42±0.03	64.74±1.26	81.82±0.39
$k = 4$	51.78±0.55	89.09±0.06	69.02±0.10	82.08±0.07	70.24±0.24	81.58±0.02	63.70±0.66	82.10±0.20
	ODIN							
$k = 1$	54.09±1.52	90.04±0.32	59.67±0.75	86.47±0.44	63.73±0.79	84.74±0.28	55.95±1.69	85.81±0.64
$k = 2$	50.17±0.63	91.44±0.16	57.59±0.37	87.53±0.07	61.73±0.36	85.87±0.09	51.64±1.32	87.81±0.37
$k = 3$	48.96±0.84	91.79±0.08	57.15±0.21	87.64±0.20	61.11±0.12	86.04±0.05	49.95±0.98	88.24±0.31
$k = 4$	47.72±0.57	92.03±0.05	56.48±0.33	87.91±0.03	60.75±0.09	86.25±0.06	49.37±0.35	88.50±0.18
	Energy							
$k = 1$	57.14±1.45	89.38±0.32	57.78±1.05	86.75±0.47	62.56±0.64	84.83±0.31	54.18±1.72	86.03±0.66
$k = 2$	53.40±0.80	90.86±0.20	55.46±0.59	87.57±0.24	60.02±0.07	85.82±0.12	48.66±0.88	88.07±0.50
$k = 3$	52.00±0.67	91.34±0.07	54.02±0.18	88.18±0.13	59.44±0.25	86.38±0.06	46.81±0.56	88.92±0.15
$k = 4$	51.75±0.24	91.51±0.04	53.93±0.27	88.26±0.13	59.20±0.15	86.44±0.09	46.09±0.48	89.03±0.18
	GradNorm							
$k = 1$	56.87±4.22	83.87±1.71	64.23±2.37	79.38±1.15	72.42±1.49	75.28±0.86	60.02±2.96	79.25±1.23
$k = 2$	52.67±1.41	86.14±0.48	61.02±1.14	81.14±0.52	69.99±0.99	77.02±0.40	56.49±2.46	81.67±1.20
$k = 3$	53.24±1.57	86.16±0.59	61.28±0.93	81.25±0.42	69.85±0.52	77.27±0.31	56.82±1.16	82.11±0.62
$k = 4$	50.73±0.80	87.15±0.27	60.08±0.54	81.89±0.20	69.02±0.40	77.83±0.15	55.57±0.28	82.63±0.24
	Mahalanobis							
$k = 1$	96.74±1.01	51.44±5.63	96.84±0.39	50.57±2.00	96.29±0.37	51.84±1.10	43.02±7.89	78.30±8.48
$k = 2$	97.14±0.56	51.22±5.08	97.00±0.28	50.83±0.39	96.43±0.44	53.10±1.16	44.04±7.50	77.34±8.22
$k = 3$	97.44±0.18	49.69±2.56	97.03±0.06	51.37±0.42	96.21±0.25	54.42±0.46	46.74±3.58	74.65±4.21
$k = 4$	97.46±0.26	51.52±0.86	97.24±0.19	51.04±0.96	96.58±0.21	53.78±0.84	43.83±0.45	78.34±0.54
	RankFeat							
$k = 1$	87.91±8.24	63.17±11.47	82.25±6.77	73.38±7.74	85.79±5.13	68.94±6.86	63.83±9.05	79.96±5.41
$k = 2$	81.78±12.13	65.91±13.15	75.24±7.78	77.17±4.21	80.77±5.67	71.95±3.88	48.51±12.19	87.40±4.45
$k = 3$	81.49±3.89	67.76±5.56	68.66±5.92	80.83±3.01	75.58±3.89	75.22±2.65	40.32±5.00	90.61±1.64
$k = 4$	76.87±4.21	71.93±3.41	64.03±5.12	82.46±2.24	72.72±3.74	76.68±2.05	35.14±3.36	92.16±0.89

Table IV.11: The detection performance of ensembling k modes (**ResNet50** trained on **ImageNet**) on each OoD data set *w.r.t* different types of OoD detectors. The results with the **lowest variances** are highlighted with bold fonts.

Ensemble of k modes	OoD data sets							
	iNaturalist		SUN		Places		Textures	
	FPR↓	AUROC↑	FPR↓	AUROC↑	FPR↓	AUROC↑	FPR↓	AUROC↑
	MSP							
$k = 1$	58.38±1.87	86.99±0.45	70.41±0.93	80.96±0.32	72.70±1.17	80.01±0.37	66.32±1.29	80.62±0.26
$k = 2$	54.69±1.01	88.29±0.24	68.75±0.39	82.03±0.04	70.72±0.37	81.21±0.12	64.05±0.57	81.58±0.05
$k = 3$	53.57±0.55	88.75±0.19	68.31±0.21	82.18±0.09	70.74±0.37	81.38±0.12	63.39±0.48	81.99±0.02
$k = 4$	53.42±0.49	88.94±0.11	68.48±0.15	82.34±0.01	70.47±0.35	81.52±0.06	63.35±0.78	82.11±0.07
	ODIN							
$k = 1$	53.33±3.14	89.67±0.80	58.43±1.70	86.19±0.50	63.44±1.80	84.31±0.76	53.51±1.28	86.43±0.22
$k = 2$	50.60±2.55	91.06±0.56	56.50±1.54	87.37±0.40	61.09±0.96	85.47±0.46	49.41±0.93	88.30±0.06
$k = 3$	48.43±0.89	91.76±0.15	55.75±0.35	87.62±0.11	60.59±0.49	85.78±0.16	47.49±0.22	88.86±0.14
$k = 4$	48.37±0.28	91.93±0.09	55.81±0.50	87.74±0.14	60.62±0.46	85.89±0.20	46.52±0.57	89.13±0.08
	Energy							
$k = 1$	55.30±3.42	89.05±0.95	56.13±1.72	86.46±0.53	62.17±1.65	84.15±0.66	51.36±1.42	86.78±0.27
$k = 2$	51.33±1.78	90.85±0.46	53.75±1.14	87.64±0.22	59.90±1.54	85.44±0.48	46.00±1.18	88.83±0.11
$k = 3$	49.58±1.60	91.52±0.28	52.72±1.04	88.05±0.20	58.84±1.19	85.93±0.33	44.27±0.51	89.48±0.03
$k = 4$	49.23±0.97	91.64±0.20	52.33±0.27	88.23±0.07	58.34±0.57	86.14±0.10	42.74±0.43	89.81±0.08
	GradNorm							
$k = 1$	71.53±3.96	78.41±2.98	71.25±2.38	75.76±1.44	78.96±2.38	71.51±1.49	65.24±1.49	77.74±0.95
$k = 2$	69.97±3.93	79.96±2.53	68.72±1.53	77.06±0.94	77.15±1.67	72.93±1.08	61.93±0.88	79.85±0.41
$k = 3$	67.58±2.53	81.99±1.44	67.78±0.41	77.97±0.32	76.43±0.49	73.69±0.27	60.71±0.75	81.05±0.19
$k = 4$	67.22±1.64	82.33±0.93	66.65±0.22	78.44±0.26	75.37±0.14	74.33±0.23	59.59±0.41	81.52±0.21
	Mahalanobis							
$k = 1$	91.04±2.12	62.39±4.22	85.12±1.90	69.27±2.03	83.89±1.77	71.57±1.30	53.45±8.17	67.15±6.61
$k = 2$	88.68±2.96	65.43±2.15	83.44±3.27	72.48±4.09	83.41±2.78	73.45±2.57	44.60±8.88	75.07±5.99
$k = 3$	83.25±6.50	72.39±3.72	82.77±5.00	76.03±4.03	83.83±3.40	74.50±2.54	37.22±7.31	82.91±4.23
$k = 4$	81.49±2.78	72.42±2.48	82.59±4.45	76.15±3.11	84.14±3.55	74.44±2.07	39.01±7.63	81.81±5.44
	RankFeat							
$k = 1$	63.06±13.98	84.15±3.34	54.87±17.18	86.58±4.57	65.86±12.20	80.71±3.99	37.87±10.59	91.86±1.51
$k = 2$	49.18±13.04	89.67±2.61	45.30±11.30	89.80±2.57	59.64±8.77	83.70±2.61	23.21±2.71	95.04±0.10
$k = 3$	45.78±10.18	90.96±1.93	43.45±3.39	90.57±0.82	58.07±2.18	84.49±0.69	18.98±0.51	95.98±0.25
$k = 4$	40.92±5.41	91.82±0.99	38.68±3.01	91.51±0.52	54.84±2.31	85.38±0.49	16.44±0.77	96.43±0.36

Table IV.12: The detection performance of ensembling k modes (**DenseNet121** trained on **ImageNet**) on each OoD data set *w.r.t* different types of OoD detectors. The results with the **lowest variances** are highlighted with bold fonts.

Modes	OoD data sets							
	iNaturalist		SUN		Places		Texture	
	FPR↓	AUROC↑	FPR↓	AUROC↑	FPR↓	AUROC↑	FPR↓	AUROC↑
	MSP							
mode-1	48.22	88.99	65.21	81.89	68.26	80.15	61.72	82.45
mode-2	47.41	89.27	64.98	82.13	68.69	80.39	61.13	82.40
mode-3	44.52	89.78	65.12	81.82	67.32	80.75	61.88	82.63
AVG. single	46.72±1.95	89.35±0.40	65.10±0.12	81.95±0.16	68.09±0.70	80.43±0.30	61.58±0.40	82.49±0.12
AVG. ensemble	42.70±0.92	90.86±0.24	64.38±0.39	82.75±0.10	67.29±0.26	81.42±0.13	57.54±0.39	84.35±0.11
	ODIN							
mode-1	45.30	87.41	64.34	77.42	68.26	73.78	56.58	81.29
mode-2	44.66	88.08	64.29	78.09	69.36	74.68	56.74	81.25
mode-3	41.28	89.07	63.77	77.80	66.46	75.38	56.29	81.90
AVERAGE	43.75±2.16	88.19±0.84	64.13±0.32	77.77±0.34	68.03±1.46	74.61±0.80	56.54±0.23	81.48±0.36
ENSEMBLE	38.63±1.15	91.00±0.35	63.37±0.28	79.77±0.17	66.94±0.33	76.93±0.36	50.82±0.45	85.01±0.19
	Energy							
mode-1	57.93	81.43	73.11	69.69	76.81	64.47	58.58	78.54
mode-2	62.35	80.82	74.59	69.15	79.12	64.42	60.82	77.95
mode-3	57.47	83.55	73.06	70.37	76.06	66.72	57.62	79.39
AVERAGE	59.25±2.69	81.93±1.43	73.59±0.87	69.74±0.61	77.33±1.59	65.20±1.31	59.01±1.64	78.63±0.72
ENSEMBLE	49.00±0.74	88.20±0.43	70.37±0.28	74.26±0.22	73.55±0.38	69.95±0.55	48.39±0.20	84.76±0.26
	Mahalanobis							
mode-1	94.92	54.64	96.43	45.48	97.14	43.48	91.13	60.91
mode-2	99.64	37.76	98.23	35.07	98.84	34.48	84.06	62.94
mode-3	98.15	39.87	97.48	45.17	97.78	44.37	87.15	61.77
AVERAGE	97.57±2.41	44.09±9.20	97.38±0.90	41.91±5.92	97.92±0.86	40.78±5.47	87.45±3.54	61.87±1.02
ENSEMBLE	94.52±4.31	52.82±10.02	95.70±1.85	49.63±6.81	96.71±1.10	47.61±6.62	84.52±9.02	64.46±10.17
	RankFeat							
mode-1	63.71	85.64	74.30	75.72	74.05	74.66	67.48	75.24
mode-2	69.54	80.87	78.46	75.06	83.74	70.18	52.41	85.63
mode-3	61.25	86.64	71.18	78.52	71.55	77.38	68.05	75.98
AVERAGE	64.83±4.26	84.38±3.08	74.65±3.65	76.43±1.84	76.45±6.44	74.07±3.64	62.65±8.87	78.95±5.80
ENSEMBLE	54.06±5.83	89.33±1.03	70.91±2.56	80.19±1.58	72.19±1.20	78.17±1.01	55.77±7.63	83.15±4.02

Table IV.13: The detection performance of each of the 5 modes of **T2T-ViT-14** trained from scratch on **ImageNet** w.r.t 5 OoD detectors: MSP, ODIN, Energy, Mahalanobis and RankFeat. The **best** and **worst** results of each mode are highlighted.